Chapter 1
Theory of Quantum Light Sources and Cavity-QED Emitters Based on Semiconductor Quantum Dots

Christopher Gies, Matthias Florian, Alexander Steinhoff and Frank Jahnke

Abstract The first chapter presents from a theoretical perspective fundamentals and advances made in the field of quantum light sources and cavity-QED devices that are based on self-organized semiconductor quantum dots (QDs) as active material. We summarize key physical properties of QDs as embedded solid-state emitters and how to account for their semiconductor properties, such as carrier scattering, dephasing, and non-resonant coupling in microscopic theories. In combination with a quantization of the electromagnetic field, these models allow for a quantitative description of device properties and non-classical effects that render few-emitter microcavity systems so useful for applications in the quantum-information technologies.

1.1 Introduction

Research on quantum-optical light sources is to a large extent driven by applications in the so-called *new quantum technologies* [1], such as quantum computing, sensing, metrology, and cryptography, that rely on the preparation, use, and control of quantum-mechanical properties of matter or light. Photons are the smallest units of energy of the quantized electromagnetic field and play a central role, as they can be manipulated individually. At the same time they propagate at the speed of light, enabling the transfer of information over large distances ("flying qubits"). While laser physics has largely advanced to an applied and technological stage, applications that make use of the quantum-mechanical properties of photons are one fundamental research topic of this decade. The development of new devices demands bright, efficient, and integrable quantum light sources that easily couple into optical fibres. Neutral atoms and ions in traps, solid-state emitters such as quantum dots and defects, molecules, and even nanomechanical systems are being investigated for

All authors have contributed in equal amounts to this chapter.

C. Gies (✉) · M. Florian · A. Steinhoff · F. Jahnke
Institut für Theoretische Physik, Universität Bremen, Bremen, Germany
e-mail: gies@itp.uni-bremen.de

P. Michler (ed.), *Quantum Dots for Quantum Information Technologies*,
Nano-Optics and Nanophotonics, DOI 10.1007/978-3-319-56378-7_1

their potential, and interfacing these different approaches in terms of wavelength and bandwidth into "hybrid systems" is a key challenge of current research.

In this chapter, we present from a theoretical perspective fundamentals and advances made in the field of quantum light sources and cavity-QED devices that are based on self-organized semiconductor quantum dots (QDs) as active material. Semiconductor QDs are often regarded as artificial atoms due to the three-dimensional confinement potential leading to discrete electronic states. At a closer look, however, even QDs with only few confined electronic levels possess a large number of multi-exciton configurations due to many possibilities to accommodate excited carriers in these states. The Coulomb interaction separates many of these configurations energetically, thereby creating a large manifold of transition energies. This and the coupling of the QDs to their environment via phonons and excited carriers outside the QD result in two important phenomena, namely dephasing, and the possibility to enable the emission from a QD into a cavity mode even if its ground state transition is detuned by several meV. Both phenomena are an integral part of QD physics and distinguish their behavior from that of atoms. For the quantum-optical applications considered in this chapter that mostly rely on few or even a single emitter, they play an important role. In Chap. 2, nonresonant QD-cavity coupling is a central ingredient of the theory on resonance fluorescence.

After giving a short overview of theoretical approaches to solid-state cavity-QED and the characterization of light, this chapter contains four main topics. The wide range of emission properties that can be realized from single or few QDs in microcavities is discussed in Sect. 1.2. This includes cavity-QED lasing with few emitters and lasing in the presence of strong coupling, single-photon emission from few-QDs in a cavity, the direct generation of entangled photon pairs by cavity-enhanced two-photon emission, and single-photon generation with long electrical excitation pulses. In Sect. 1.3 we analyze in detail carrier scattering and dephasing processes. Section 1.4 addresses different physical mechanisms of non-resonant QD-cavity coupling. In Sect. 1.5 the role of radiative inter-emitter coupling giving rise to superradiance in QD nanolasers is discussed. It is complementary but related to the single-photon superradiance of Sect. 5.3, and both effects can strongly enhance the light-matter interaction in QD-based systems.

1.1.1 QDs Coupled to the Quantized Light Field

A central element of the theoretical description is the Jaynes–Cummings interaction of the electronic QD excitations with the quantized electromagnetic field. In atom-like systems, one typically considers a few-level model, where the electronic transitions between two selected levels is resonantly coupled to the cavity field. In QDs, the light field interacts with the multi-exciton states. These are formed from the discrete single particle states (which are the result of the three-dimensional confinement potential) and the many-body Coulomb configuration interaction.

For a small number of discrete electronic transitions, which are coupled to the Fock states of a single-mode cavity field, the Hilbert space of this system is small enough that it is possible to describe the full quantum dynamics in terms of matrix elements of the statistical operator $\rho(t)$, which follows the von Neumann-Lindblad equation,

$$\frac{\partial}{\partial t}\rho = -\frac{i}{\hbar}[H, \rho] + \sum_X \mathscr{L}_X(\rho)\,. \tag{1.1}$$

In H enters the Jaynes–Cummings Hamiltonian,

$$H_{JC} = \sum_i g_i \left(b^\dagger \sigma_i^- + \sigma_i^+ b\right)\,, \tag{1.2}$$

where $b^\dagger$ and b are creation and annihilation operators for photons in the cavity mode, $\sigma_i^\pm$ are raising and lowering operators for the electronic excitations, and g_i is the corresponding light-matter coupling strength.

When the QD is weakly excited, it is usually sufficient to consider only optical transitions between the ground state and the energetically lowest exciton state, or the biexciton to exciton to ground-state cascade. In this case, the QD-basis consists of a small set of multi-exciton states, and in the Hamiltonian $H = H_0 + H_{JC}$, the free part H_0 contains the multi-exciton energies while in H_{JC} the operators $\sigma_i^\pm$ describe transitions between different multi-exciton configurations i. Such an approach has been used, e.g., in [2–6].

At stronger pumping, several excited carriers can be present in the QD confinement potential, and their Coulomb configuration interaction leads to a large number of possible multi-exciton states. Furthermore, at higher excitation of the system, typically additional excited carriers reside in the delocalized QD barrier states. This environment leads to two important effects. The many-body Coulomb interaction between the QD carriers and the excited charge carriers outside the QD results in dephasing processes. Dephasing is also present due to the interaction of the QD carriers with phonons. Secondly, excited charge carriers outside the QD are responsible for screening of the Coulomb interaction, thus changing the configuration interaction of the QD carriers.

To describe such a situation, it is more suitable to use as basis states the many-particle configurations formed from products (Slater determinants) of single-particle states. Then the multi-exciton states follow from explicitly including the Coulomb interaction H_{Coul} in the Hamiltonian $H = H_0 + H_{Coul} + H_{JC}$ of (1.1). In this case, $\sigma_i^\pm$ describe transitions between different product states. Screening of the Coulomb interaction and the resulting dynamical changes of the multi-exciton configurations can be treated via the time dependent solution of (1.1). When including the Hamiltonian for the full QD-carrier Coulomb interaction, the Jaynes–Cummings interaction among multi-exciton states is obtained. The corresponding approach has been used in [7–9] and is the basis for various investigations discussed in this contribution.

The last term in (1.1) describes dissipation due to the coupling of the system of QD excitations and cavity photons to their environments. Here, X labels all possible transitions taking place in the system assisted by such interaction processes. Losses of cavity photons, in this chapter denoted by the rate κ, can be described via a coupling of the cavity mode to a bath of external modes [10]. Similarly, the spontaneous recombination of QD excitations into a quasi-continuum of lossy modes can be considered [10]. More challenging is the inclusion of semiconductor models for QD-carrier scattering and the resulting dephasing. How this can be realized and under which assumptions the carrier-phonon interaction and the Coulomb interaction with carriers in delocalized states can be cast into the form of Lindblad terms is the topic of Sect. 1.3. Also, the non-resonant QD-cavity coupling via many-body interaction can be described in this way, as discussed in Sect. 1.4.

1.1.2 Characterization of Light

In many experiments with semiconductor QDs in optical resonators it became customary to characterize the cavity field in terms of correlation properties of photons. Here one can distinguish between classical emission properties, like the intensity $\langle n \rangle$ (zero-order correlations) or coherence properties of the emission (first-order correlations). True quantum properties can be revealed in the intensity-autocorrelation function (second-order correlations) and in higher-order correlation functions [11].

The normalized first-order correlation function,

$$g^{(1)}(t,\tau) = \frac{\left\langle b^\dagger(t)\, b(t+\tau)\right\rangle}{\left\langle b^\dagger(t)\, b(t)\right\rangle}, \tag{1.3}$$

describes field-amplitude correlations as measured with a Michelson interferometer. In a stationary situation, when $g^{(1)}$ is independent of t, the coherence time of the radiation is given by

$$\tau_c = \int_{-\infty}^{\infty} d\tau \ \left|g^{(1)}(\tau)\right|^2 \tag{1.4}$$

and the emission spectrum follows from a Fourier transform of $g^{(1)}(\tau)$:

$$S(\omega) = \frac{1}{2\pi}\int_{-\infty}^{\infty} d\tau\ e^{-i\omega\tau} g^{(1)}(\tau). \tag{1.5}$$

Information on statistical properties of the radiation are contained in the second-order, or intensity autocorrelation function,

$$g^{(2)}(t,\tau) = \frac{\left\langle b^\dagger(t)\, b^\dagger(t+\tau)\, b(t+\tau)\, b(t)\right\rangle}{\left\langle b^\dagger(t)\, b(t)\right\rangle \left\langle b^\dagger(t+\tau)\, b(t+\tau)\right\rangle}. \tag{1.6}$$

In a stationary situation, $g^{(2)}(\tau = 0)$ can be used to identify thermal radiation, for which $g^{(2)}(0) = 2$, indicating high likelihood of finding two photons at the same time (photon bunching). This can be distinguished from coherent radiation obeying Poisson statistics, where $g^{(2)}(0) = 1$. This situation is realized in an ideal laser, where the only noise arises from the randomness of spontaneous emission. For nonclassical light the intensity correlation is $g^{(2)}(0) < 1$ (photon antibunching).

If the system is driven by an excitation pulse, no stationary state exists, and the correlation functions are explicitly t-dependent. It is straightforward to calculate $g^{(2)}(t, \tau = 0)$ e.g. by evaluating the expectation value from the time-dependent density operator, see Sect. 1.5. Delay-time τ dependent results can be obtained with the help of the quantum regression theorem [12]. In a density-matrix approach, this procedure is explained in detail in [13]. The spirit of the quantum-regression theorem can be transfered to hierarchies of equations that are obtained by cluster-, or correlation-expansion methods [14–19] to obtain $g^{(1)}(t, \tau)$ [20, 21] and $g^{(2)}(t, \tau)$ [20]. The calculation of $g^{(2)}(\tau)$ under pulsed excitation conditions is more intricate and requires averaging over a multitude of two-time calculations [22].

Finally, we point out the link between the second-order photon correlation function and the photon-number probability distribution function (a.k.a. photon statistics) p_n, which refers to the diagonal elements of the photon density matrix after the electronic degrees of freedom have been traced out. For equal-time operators, (1.6) can be rewritten as

$$g^{(2)}(t, \tau = 0) = \frac{\langle n^2(t)\rangle - \langle n(t)\rangle}{\langle n(t)\rangle^2}, \tag{1.7}$$

where $\langle n(t)\rangle = \langle b^\dagger(t)b(t)\rangle$. As the photon operators act only on the photonic degrees of freedom, in this representation it is straightforward to see that $\langle n\rangle$ and $\langle n^2\rangle$ are the first and second moments of the photon statistics, respectively. While a distribution function can be accurately represented by *all* of its moments, the autocorrelation function $g^{(2)}(t, \tau = 0)$ therefore contains only partial information on the full photon statistics. As such, an interpretation of $g^{(2)}(t, \tau = 0)$ requires at least some intuition about the underlying distribution function, otherwise results can be misleading. We give an example in Sect. 1.2.1.

1.2 Emission of Single and Few-QD Microcavity Systems

The discrete level structure and tunability of the electronic properties of semiconductor QDs can be exploited to design deterministic quantum-light sources. A single QD driven with short optical excitation pulses produces antibunched single photons on demand [23], the demonstration [24] of which has played a great part to promote solid-state systems into the quantum-information research field. The fabrication of nanostructures, where a single QD is embedded in a microresonator, offers particular advantages for applications both in quantum-information technologies and lasers. The confinement of the light field can be used to enhance the emission from

Table 1.1 Different operational regimes of single or few QDs in optical cavities and the quantities used to characterize the quantum-optical properties of the emission. The last point in the list refers to [27]

Operational regime:	*Characterisation:*
Lasing in weak coupling regime *(1-many QDs)* medium to strong excitation	$g^{(2)}(0) = 1$, $\langle n \rangle > 1$, increase in coherence time
Lasing in strong coupling regime *(1 QD)* high ratio of g/κ, low to medium excitation	$g^{(2)}(0) = 1$, footprints of higher excited states in emission spectrum
Sub- and superradiant emission *(2-1000 QDs)* QD-QD coupling via light field	super-thermal $g^{(2)}(0) \gg 2$, faster spontaneous emission
Single-photon emission *(1 QD)* no cavity or low-Q cavity, weak excitation	$g^{(2)}(0) \cong 0$, Hong-Ou-Mandel
Cavity-enhanced single-photon emission *(1-few QDs)* right balance between cavity losses, strong excitation	error/purity η of single-photon emission
Cavity-selected entangled-photon-pair emission *(1 QD)* high-Q cavity tuned to two-photon resonance	concurrence, fidelity, $g^{(2)}(0) > g^{(2)}(\tau > 0)$
N-photon Fock-state emission *(1 QD)* strong light-matter coupling, detuned excitation	time-ordered $g^{(2)}$

transitions between QD many-particle configurations, promising higher repetition rates for single-photon sources and smaller losses for high-efficiency lasers. At the same time, the cavity acts as a spectral filter and introduces the Jaynes–Cummings nonlinearity, enabling the use of effects like the photon blockade [25, 26]. The surprisingly diverse range of regimes in which QD-microcavity systems can operate may be fascinating and confusing at the same time. Table 1.1 is an attempt to provide an overview.

1.2.1 Single Photons from a Single and Few QDs in a Cavity

A typical single-photon source is realized without a cavity, or with a weakly-reflecting mirror to enhance the emission directionality. More recent technological advances have enabled the fabrication of microresonators that contain exactly one QD emitter in the field maximum of a single mode [28], allowing to use the benefits of cavity-QED effects for the design of single-photon sources [29–31].

The emission properties of a single QD in a cavity can vary from single-photon emission to lasing [7, 8, 32, 33]: In the low-Q cavity regime antibunched emission ($g^{(2)}(0) = 0$) of the single QD dominates. On the other hand, high-Q cavities with photon losses on ps timescales enable the accumulation of photons such that the single emitter can be driven close to or even into the regime of lasing, where coherent emission results from a Poissonian cavity light field. In the left panel of Fig. 1.1

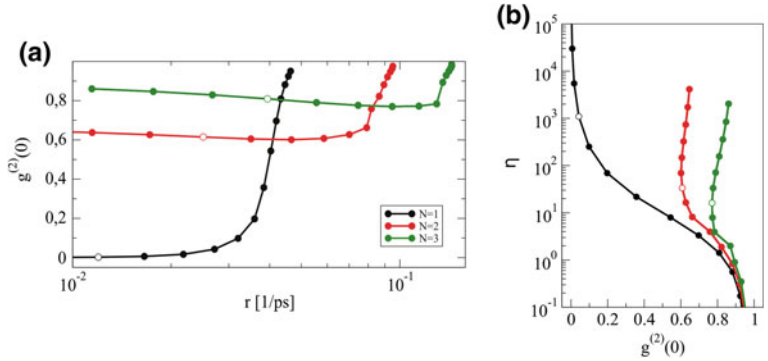

Fig. 1.1 **a** Autocorrelation function $g^{(2)}(0)$ as a function of the photon output rate for N = 1, 2, 3 emitters. Each *curve* is obtained from a series of calculations where the cavity-Q is varied. From *left* to *right*, κ = 10, 6.3, 4, 2.5, 1.6, 1, 0.63, 0.4, 0.25, 0.16, 0.1, 0.063, 0.04, 0.025, 0.016, 0.01/ps, *open circles* indicate κ = 2.5/ps on each *curve*. High excitation is used to drive the system into saturation. **b** Single-photon purity η versus $g^{(2)}(0)$. Starting from high η, the same values for κ are used, *open circles* indicate κ = 0.63/ps on each *curve*

we classify these two regimes as a function of the maximally attainable emission rate $r = \kappa\langle n\rangle$. Using strong incoherent excitation, each symbol on the black curve represents a single-QD-microcavity system with a unique cavity loss rate κ. To the left side one approaches the limit of a free QD emitter (large κ). To the right side, the cavity losses become smaller than the spontaneous emission rate, so that photons accumulate in the cavity and lead to coherent emission with $g^{(2)}(0) = 1$. In between, there is a wide regime with cavity-enhanced single-photon emission, where $0 < g^{(2)}(0) < 0.5$. In the solid-state community, this is a frequently used criterion to identify the source of the emission to be a single emitter, since the smallest possible $g^{(2)}(0)$ value from a two-emitter system is that of a two-photon Fock state yielding 0.5.

How do additional emitters influence this result? Non-resonant coupling of spectrally detuned QD transitions to the cavity mode distinguishes solid-state emitters from atoms (cf. Sect. 1.4). Most current realizations of SQD nanostructures are not free of residual emitters [32, 33]. When comparing to experiments, background effects from detuned emitters can play an important role and significantly modify the properties of a true single-emitter system. While it may seem intuitively clear that a single-photon source can only be realized using a single-emitter, this is not entirely true if the cavity acts as a filter for the statistical properties of photons originating from *several* emitters, or if these emitters are correlated in an entangled state. In the left panel of Fig. 1.1 results are also shown for two and three emitters in the cavity. Surprisingly, non-classical emission is also possible, even if perfect antibunching in terms of $g^{(2)}(0)$ values being as close as possible to zero is compromised in comparison to the single-emitter case. We take a closer look at the interpretation of these results, first reminding ourselves that according to (1.7), $g^{(2)}(0)$ contains information from the photon statistics in an averaged form via the first and second *moments* of

the probability distribution function p_n. The performance of a single-photon source is more accurately characterized in terms of the rate r (how long on average must one wait for an emission event) and the error η^{-1} to have an unusable packet with more than one photon. This characterization can be realized if access to the full photon statistics is available, such as from density-matrix calculations or photon-number resolved measurements. We define the single-photon purity (inverse to the error) as

$$\eta = \frac{p_1}{\sum_{i\geq 2} p_i} \tag{1.8}$$

that relates the probability of the emission of a single photon to that of the emission of bundles of two or more photons [34, 35]. Single-photon purity is one of the criteria listed in Chap. 3 Sect. 2, to which we refer for further information on single-photon sources. In the right panel of Fig. 1.1 we show the attainable η and the corresponding $g^{(2)}(0)$ for the κ values used in the left panel. While the error can only be arbitrarily minimized in the single-emitter system, high η can also be obtained with two and three emitters in the cavity. Most interestingly, the autocorrelation function is unable to capture this behavior, as for the same purity of single-photon emission, $g^{(2)}(0)$ values can be very different. Moreover, the same high η may be achieved with higher emission rates from two and three emitters [34]. The impact of additional emitters in the cavity can apparently be less detrimental than one may expect from $g^{(2)}(0)$ alone. In the future, it will be very interesting to further investigate emission properties beyond the well-established autocorrelation measurements on the basis of photon-number resolving detectors [36–40] or higher-order HBT setups [41].

1.2.2 Lasing in the Presence of Strong Coupling in a Few-QD System

The miniaturization limit of solid-state cavity-QED is given by a single QD coupled to a single mode of a microcavity. In order to achieve sufficient photon production from only a single emitter, the light-matter coupling must be as high as one can achieve by using emitters with large dipole moments and by placing them in the field maximum of the confined mode. Coupling-strength values for current micropillar cavity systems are close to 100 μeV, which is sufficiently high to be in the strong coupling regime even at increased excitation powers. While strong coupling is associated with weak excitation and the appearance of the vacuum Rabi doublet in the emission spectrum, lasing typically takes place in the weak coupling regime using strong excitation. It is therefore an interesting thought that the lasing threshold is crossed while the transition of a single QD is still in strong coupling with the mode. This was first discussed in [42] for a photonic-crystal cavity containing only few QD emitters, although in the past, neither was the influence of the background emitters quantified, nor the role of excitation-induced dephasing, which is the main reason for the transition to weak coupling at higher excitation, discussed.

The criterion for strong coupling is commonly accepted as the existence of two distinguishable peaks in the cavity emission spectrum, the so-called vacuum Rabi doublet. In general, the spectrum can be written as the modulus square of the difference between two poles [43]

$$S(\omega) \sim \left| \frac{1}{\omega - \omega_1} - \frac{1}{\omega - \omega_2} \right|^2 . \tag{1.9}$$

In the presence of dephasing, such as originating from cavity losses, spontaneous emission, or carrier relaxation processes following excitation, it is known [44, 45] that strong coupling persists as long as $4g > |\Gamma - \kappa|$, where g is the light-matter coupling strength, κ the cavity loss rate, and Γ gives the total exciton dephasing, before the Rabi doublet merges into a single line marking the transition to weak coupling [10]. This well-known strong-coupling criterion must be reviewed, however, when excitation is strong enough that states with higher total excitation in the Jaynes–Cummings ladder become populated, such as when approaching the laser threshold.

A nanolaser can be seen as a driven dissipative system that is defined by the usual Jaynes–Cummings Hamiltonian and Lindblad contributions for pump, relaxation, and losses. An analytic expression for the cavity emission spectrum can only be obtained by limiting the Hilbert space to a low-excitation subspace. Using the two-level formalism for simplicity, in [10] the three lowest states, namely the ground state in the zero-photon block $|g, 0\rangle$ and the states with one excitation $|e, 0\rangle$ and $|g, 1\rangle$ (Fig. 1.2 depicts these states and their relation to the dressed-state Jaynes–Cummings ladder), are used to derive the well-known expression for the cavity spectrum. While this "three-state approximation" (3SA) sufficiently describes the strong-coupling spectrum in the weak-excitation regime, higher states become realized under stronger excitation as one begins to climb the Jaynes–Cummings ladder. In this case, we

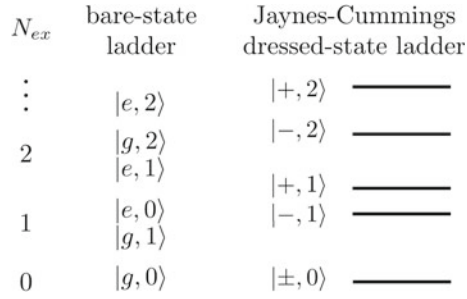

Fig. 1.2 Illustration of the implications of the 3- and 4-state approximation (SA). In the 4SA, the four lowest-energy states are explicitly considered including the state $|e, 1\rangle$ with a total excitation number of $N_{ex} = 2$. In a dressed-state picture, this allows to represent the lowest two rungs of the Jaynes–Cummings ladder and, thereby, to obtain the vacuum-Rabi doublet that results from the two possible transitions from the first rung to the ground state. The 3SA is limited to states with a maximum $N_{ex} = 1$. The Rabi-doublet is inaccurately described by the 3SA if the system pumped towards the lasing threshold, as the first JC rung cannot be represented by the $N_{ex} = 1$ states alone

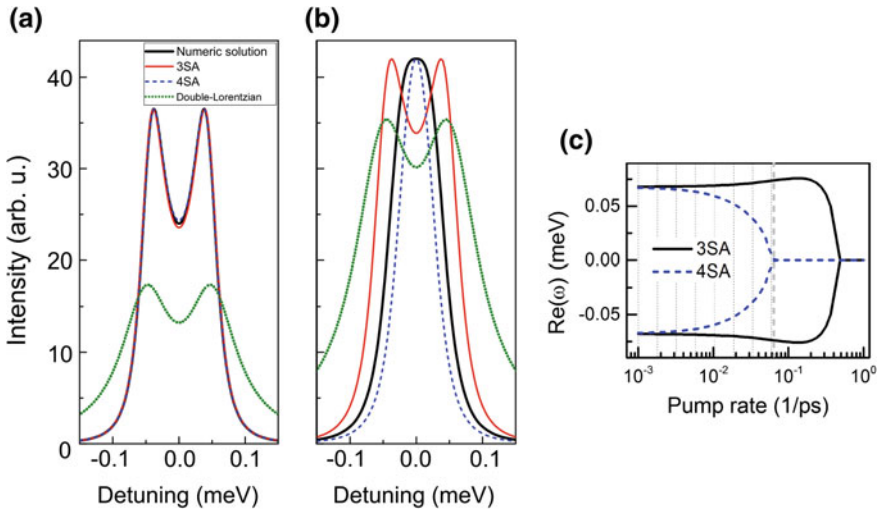

Fig. 1.3 Comparing different approximations to the cavity emission spectrum at low (**a**) and high (**b**) excitation power. **c** Real part of the poles that determine the peak positions in the 3SA and 4SA. Two separate values indicate the peak splitting of the strong regime

show that considering the next higher excited state $|c, 1\rangle$ with a total excitation of 2 extends the validity of the approximation into the transition regime to lasing. In this "four-state approximation" (4SA) the cavity emission spectrum can be written as a closed analytic expression of the form of (1.9), where the roots that determine the position of the peaks are changed by additional terms [46]. In Fig. 1.3 both levels of approximation are compared to the full numerical solution. While the additional higher excited state in the 4SA has little impact in the low-excitation regime (a), its absence can be noted at high excitation (b): The conventional 3SA textbook expression incorrectly predicts Rabi splitting, whereas the result obtained in the 4SA closely resembles the numerical result, which reveals that the transition to weak coupling has taken place. The remaining difference between the 4SA and the exact solution can be attributed to contributions from yet higher excited states. In systems that are driven with higher excitation-power densities, the 4SA-analytic formula for the cavity emission spectrum provides a new tool to evaluate experimental measurements and to extract parameters, such as the light-matter coupling strength, with greatly improved accuracy.

In Fig. 1.3c the eigenvalues that determine the peak-positions in the emission spectrum are compared for 3SA and 4SA. One can infer that the transition to weak coupling, indicated by the merging of the poles, takes places at much higher excitation-induced dephasing (i.e. higher pumping) if the approximation is restricted to only the three lowest states. This finding has severe implications for answering the question if lasing and strong coupling can coexist.

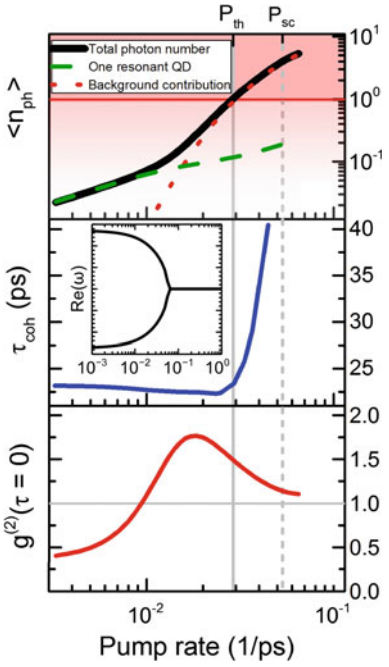

Fig. 1.4 Laser characteristics obtained from a numerical solution of a density-matrix approach that includes contributions from background emitters. From *top* to *bottom*, input-output curve, coherence time and second-order photon correlation function are shown, in their combination providing evidence that the system is a nanolaser that crosses the transition to lasing

As discussed in Sect. 1.1.2, the photon autocorrelation function $g^{(2)}(0)$ approaching unity is indicative for lasing, and so is a linewidth narrowing that begins to take place at the laser transition [47]. In Fig. 1.4 we show numerical results for both quantities together with the input-output curve. The calculation takes into account a single QD that is in strong coupling with the mode (see the inset) and several "background emitters" which only come into resonance at higher excitation. The underlying picture is that their exciton transition is detuned from the cavity mode, but transitions between higher multi-exciton states that become realized at stronger excitation are resonant. Non-resonant coupling via multi-exciton states is explained in Sect. 1.4.2 of this chapter. From the top to the bottom panel, we see a kink in the input-output curve that originates from background contributions (dotted curve) to the emission of the single QD (dashed curve). A mean intracavity photon number of 1 is reached at $P_{th} = 0.02$/ps. At this value, the coherence time shows a steep increase to moderately low values reaching 40 ps. The low coherence time reflects the significant fraction of spontaneous emission also in the lasing regime due to the small overall number of emitters. In contrast, in a many-emitter laser, spontaneous emission plays practically no role above threshold, and the coherence time can be 1 ns [21]. The autocorrelation function exhibits antibunching ($g^{(2)}(0) < 1$) of the strongly coupled single emitter in the low excitation regime. Antibunching disappears with the onset of contributions from the additional QDs, where spontaneous emission of their various emission channels leads to a thermal component ($g^{(2)}(0) > 1$). At high excitation, coherent lasing with $g^{(2)}(0) = 1$ is be reached.

These results are representative for the behavior of a few-emitter QD-microcavity system, which can operate in a variety of regimes depending on system parameters and excitation strength thereby crossing between single-emitter behavior, LED emission, and lasing in different regimes of light-matter coupling. An understanding of the intricate behavior requires to use a quantum-optical framework that takes into account a variety of effects that are fundamentally relevant for solid-state emitters and that are discussed in this chapter, such as non-resonant coupling, excitation-induced dephasing, and multi-exciton transitions.

1.2.3 Cavity-Enhanced Emission of Entangled Photon Pairs

Pairs of entangled photons are essential to many building blocks for quantum technologies. This includes quantum repeater stations that are needed to extend quantum communication networks beyond the limitations due to losses in optical fibres [48], as well as quantum teleportation and key distribution via the E91 protocol [49]. Today's applications mostly rely on parametric downconversion in non-linear crystals to generate entangled photons. Semiconductor QDs possess particular properties that make them promising candidates for integrated deterministic sources of entangled photons. The following discussion refers to the energy scheme in the left panel of Fig. 1.5. Prepared in the biexciton state, two decay channels are equally possible, in which an electron-hole pair of either spin direction recombines and leaves behind a remaining exciton with an electron and a hole of the opposite spin (X_H or X_V), emitting a photon that is either horizontally or vertically polarized. From there a second recombination is possible, resulting in the emission of another photon of the same polarization as the first one. If both intermediate exciton states are energetically indistinguishable, the "which-way" information is not revealed, and the result is the entangled photon state $(|HH\rangle + |VV\rangle)/2$, where $|12\rangle$ denotes the two-particle state of the two-photon system.

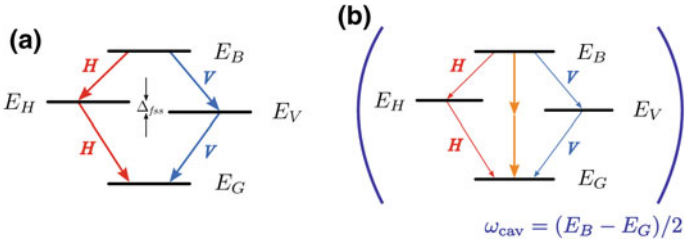

Fig. 1.5 **a** With energy displayed along the vertical direction, the so-called 'diamond' scheme of the biexciton-to-ground-state cascade of a semiconductor QD is schematically depicted. The intermediate excitonic states are energetically separated by the fine-structure (fss) splitting. **b** Emission of an entangled photon pair by cavity-enhancement of a direct two-photon emission process

Unfortunately, due to growth-related anisotropies, both excitons are not indistinguishable, but energetically separated by the fine-structure splitting (fss). The possibility to distinguish the two recombination channels by their spectral footprint provides the "which-way" information that compromises entanglement. Many attempts have been undertaken to minimize the fss, e.g. by applying external electrical fields or doping [50], and we refer the reader to Chap. 7 for a detailed discussion. We propose an elegant alternative approach that avoids the detrimental effect of the fss altogether.

In [3] the direct two-photon emission process from the biexciton to the ground state is employed, from which each photon carries half the energy of the biexciton. As higher-order process that is of second order in the Hamiltonian, the two-photon emission is as such highly unlikely and hardly relevant in previous discussions of biexciton emission of entangled photon pairs. If, however, the emitter is embedded in a cavity that is tuned exactly to the energy of the two-photon emission, the modified photonic density of states enhances the two-photon emission and suppresses emission through the cascade. This situation is depicted in the right panel of Fig. 1.5. Both processes compete with each other, and it depends sensitively on the parameters, in particular on width (Q-factor) and position of the cavity mode, whether entanglement can be preserved in the presence of fss.

For sufficiently high (but also typical) cavity-Q factors of about 20,000, we could demonstrate nearly complete independence of the degree of entanglement on the fss as shown in the left panel of Fig. 1.6. In the right panel, it is shown that in case of perfect resonance between cavity and two-photon emission process, the delay-time resolved autocorrelation function $g^{(2)}(\tau)$ exhibits bunching at $\tau = 0$, revealing that both photons are indeed most likely emitted simultaneously. If the cavity is detuned only slightly (0.25–0.5 meV) from that resonance, the bunching peak moves away

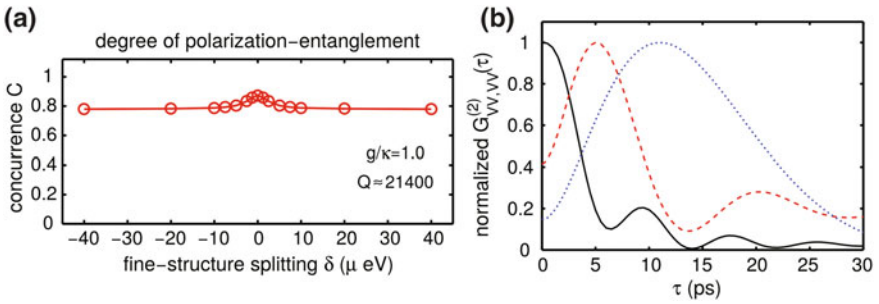

Fig. 1.6 **a** The degree of polarization entanglement (C = 1 representing a maximally entangled state) remains nearly constant as function of fine-structure splitting, if a Q = 21400 cavity mode is tuned exactly to the two-photon resonance of the biexciton transition. **b** The fingerprint of the two-photon emission is a bunching-peak in the two-photon correlation function at zero time delay, whereas emission through the biexction-exciton-ground state cascade exhibits bunching at a delayed time. In resonance (*solid curve*), two-photon emission is enhanced by the cavity and is the dominant process. For slight detuning (0.25 meV *dashed*, 0.5 meV *dotted curve*), emission through the cascade becomes increasingly more likely, indicated by the peak moving away from $\tau = 0$

from the origin $\tau = 0$, indicating that the two photons are emitted successively and the emission mechanism shifts from the direct higher-order process to the cascade.

An experimental verification of the feasibility of the proposed generation of a quantum-mechanical entangled state is yet to be provided. Both the direct creation of the biexciton state by a direct two-photon *absorption* process [51], and the possibility of the discussed two-photon emission process (although in the absence of a cavity) [52] have recently been demonstrated.

1.2.4 Single Photons from an Electrical Source with Long Pulses

As a final example for the generation of non-classical light we consider a single emitter without the influence of a cavity. In the experimental realization [53], a bottom DBR-mirror is used merely to enhance directionality of the emission.

The repetition rate of an on-demand single-photon source is limited by the recombination time of the emitter. When using short (picosecond) excitation pulses with sufficient temporal separation, each pulse triggers a single-photon emission event. The duration of the excitation pulse must remain shorter than the average recombination time in order to avoid re-excitation following the same trigger, which would result in the emission of successive photons. While short excitation pulses are easily realized in all-optical setups, electrical excitation by current injection is the device-relevant method of excitation and one key advantage of solid-state emitters over atomic systems. Picosecond-short excitation pulses are, however, more difficult to realize with electric pulse generators. Addressing this problem, we have proposed an excitation scheme that makes use of the multi-exciton landscape of QD excitations to realize strongly antibunched single-photon emission that is quite independent of the excitation-pulse duration [53].

Instead of using weak excitation pulses, the pump pulses are chosen strong enough to drive the system into saturation. Consequently, during the excitation the QD is rapidly filled with carriers and the emission is dominated by the recombination of higher multi-exciton configurations, which are spectrally detuned from the exciton-to-ground-state transition. After the excitation pulse has ended, carriers recombine until no carriers remain in the QD. The last decay in this cascade must result from the neutral or charged exciton with only one remaining electron-hole pair at a unique spectral position. It is the basic idea of the proposed scheme to trap the system in higher multi-exciton configurations *during* the excitation and to use spectral filtering to collect the single photon from the final exciton emission *after* the excitation pulse has ended. The detuned emission during the excitation is not collected, and the final exciton emission is independent of the duration of the excitation pulse. The dynamical behavior of this interplay of different recombination channels is depicted in Fig. 1.7 (theory in (a), experiment in (b)). As a central result, by using strong excitation a high degree of antibunching with $g^{(2)} < 0.1$ can be maintained quite

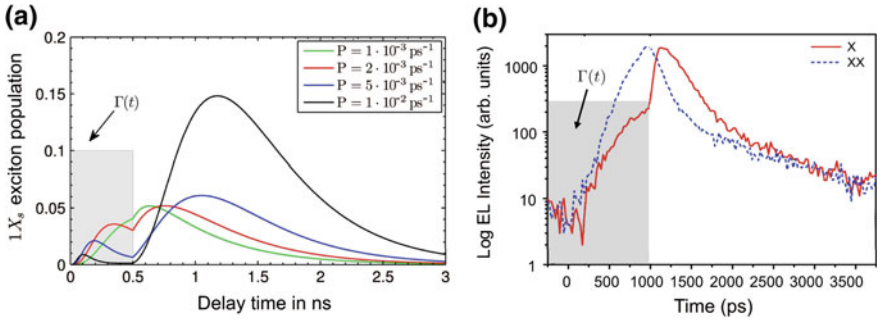

Fig. 1.7 **a** Time-dependence of the exciton realization probability following pulsed excitation of different excitation powers. The realization of the exciton configuration is suppressed with increasing pulse area of the excitation, as higher multi-exciton configurations form instead. After the pulse has ended, the exciton is realized and then decays on the typical nanosecond timescale. **b** Time-resolved measurements of the exciton (X) and biexciton (XX) emission intensity. In agreement with the microscopic model, during excitation exciton emission is suppressed and emission from the biexciton dominates. After the excitation pulse, the exciton transient reflects the theoretically predicted behavior. The duration of the excitation pulse $\Gamma(t)$ is indicated by the *shaded region*. Note the different scales (*top*: linear, *bottom*: logarithmic) when comparing the results. The *left figure* is taken from [22], the *right figure* is adapted from [53]

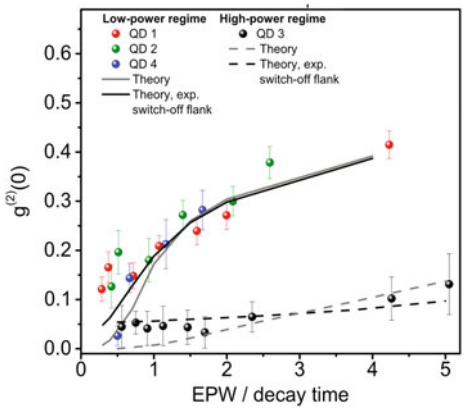

Fig. 1.8 Antibunching quantified in terms of $g^{(2)}(0)$ as function of the width of the electrical excitation pulse (EPW)

independently of the excitation-pulse duration, as shown in Fig. 1.8. Experimentally, this has been verified for nanosecond pulse durations exceeding the recombination time by more than 500% in excellent agreement with the theoretical results obtained from a solution of the von-Neumann equation [22].

1.3 Carrier Scattering and Dephasing

In solid-state physics, we usually deal with systems exhibiting a continuous density of states, where the full quantum dynamics of excited carriers is practically not accessible and theories have to be formulated in terms of averaged one- or two-particle quantities. On the other hand, semiconductor quantum dots (QDs) are quasi-atomic systems with a discrete spectrum of confined states, where the dynamics of the full density operator can be calculated via a von Neumann equation, as discussed in the introduction to this chapter. Unlike true atoms, QDs are not isolated but embedded into a semiconductor crystal and have to be treated as open quantum systems in interaction with their environment of lattice vibrations and charge carriers of the barrier material as well as the photon modes of free space. The dissipative processes, in particular carrier-carrier and carrier-phonon interaction, are typically described by many-particle methods that can be formulated such that the coherent von Neumann dynamics is supplemented by additional Lindblad terms, as we show below.

The density operator $\rho(t)$ of the QD system is expressed in a basis of many-particle states. This leads to a full description of the QD excitations, in which the Coulomb interaction of QD carriers can be directly included. As mentioned in the introduction, there are basically two ways to construct the many-particle basis and formulate the dynamics of the density operator. On the one hand, we can start from the single-particle states that are provided by the QD confinement potential and build many-particle configurations, or product states, by creating carriers in the single-particle states in all possible combinations. A given configuration $|\{n_i\}\rangle$ is then defined by specifying which single-particle states are occupied ($n_i = 1$) or empty ($n_i = 0$). The Coulomb configuration interaction can be included in the Hamiltonian of the von Neumann equation, thereby considering the formation of multi-exciton states, which are the fundamental QD excitations. Alternatively, we can take into account the configuration interaction in advance and select an appropriate set of multi-exciton states as a basis for the density operator, which is often done in quantum optics to formulate compact models of QD emitters. In this section, we will follow the first approach and stay with product states as the many-particle basis as discussed in [9].

The electronic many-particle basis can be augmented by photonic degrees of freedom to capture the full quantum dynamics of QD emitters inside a cavity. In this section, we focus on carrier scattering and dephasing by treating the electronic part of the density operator ρ_{el}. We can describe the dynamics of ρ_{el} by the von Neumann-Lindblad (vNL) equation [54–56]

$$\frac{\partial}{\partial t}\rho_{\mathrm{el}} = -\frac{i}{\hbar}\left[H_S, \rho_{\mathrm{el}}\right] + \sum_X \frac{\gamma_X}{2}\left[2s_X\rho_{\mathrm{el}}s_X^\dagger - s_X^\dagger s_X\rho_{\mathrm{el}} - \rho_{\mathrm{el}}s_X^\dagger s_X\right]. \tag{1.10}$$

The commutator part represents the coherent time evolution of the density operator due to the system Hamiltonian H_S, which consists of a "free" part with the QD confinement energies and the Coulomb interaction between the QD carriers. It defines the eigenenergies of the QD many-electron system and takes into account

all Coulomb renormalization effects caused by the interaction of QD carriers among each other. By accounting for the interaction between the QD system and its semiconductor environment, which is formally described by a number of reservoirs, the so-called Lindblad terms are obtained. They introduce dissipation into the time evolution, causing the QD to relax to a thermal equilibrium which is defined by the properties of the environment. This also includes interaction-induced dephasing of coherences that may be generated in the QD for example by light-matter interaction. The summation in (1.10) runs over all possible transitions between the eigenstates of the QD, the transitions being described by operators s_X. It is essential that both the interaction of QD carriers with phonons and with charge carriers of the barrier material can be formulated as Lindblad terms, where the transition rates γ_X can be calculated microscopically. But even if we choose phenomenological values of γ_X that are e.g. based on experimental results instead of a microscopic calculation, the structure of the vNL equation guarantees physically sensible results.

Due to their direct relevance for various QD applications, in the past two decades carrier-scattering processes in QD systems have been studied intensively both in experiment [57–63] and theory [64–74]. A microscopic description of carrier scattering requires the inclusion of carrier correlations that can be treated on different levels. For QD systems, due to the finite state space of the electronic excitations, approximate treatments of carrier correlations have been questioned and the importance of a configuration picture has been pointed out. [16] Consequences for QD laser threshold current densities, [75] or QD gain recovery dynamics [76] have been demonstrated. Moreover, a carrier-capture model consisting of several capture configurations in the QD has been used to explain signatures of a phonon bottleneck in time-resolved differential transmission measurements on InGaAs quantum dots [58]. In [77], the effect of full Coulomb configuration interaction on the carrier relaxation in weakly confined QDs due to electron-acoustic phonon interaction has been discussed. The description in terms of a many-particle basis, which is naturally chosen for quantum optical models of QD emitters, is complemented by the description of carrier scattering on a single-particle level, which is often used throughout the literature. Again, it is questionable if a single-particle description of carrier scattering may be used in QD systems with a small number of electronic states, as we illustrate in the following.

When the vNL equation (1.10) is used, relaxation processes occur as transitions between QD configurations, facilitating an exact treatment of the Pauli exclusion principle between the QD carriers. In a single-particle description, for example in terms of a Boltzmann equation, the central quantities are the occupation *probabilities* f_i of the single-particle states. These describe the population of a QD in the sense of an ensemble average, which corresponds to each carrier reacting not to the actual state of the collision partners in a scattering process, but to an independently averaged "mean-field" distribution of carriers, see Fig. 1.9. As discussed in [9], this corresponds to a mean-field-like treatment of Pauli blocking, which can lead to inaccurate results in the description of carrier relaxation: If the QD is prepared in a state where only one efficient relaxation channel is available, only one Lindblad term is present in (1.10), exhibiting a purely exponential time evolution with a constant rate due to the linear

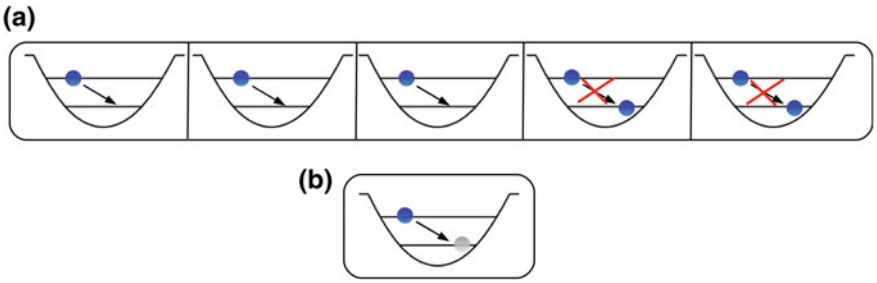

Fig. 1.9 Schematic of carrier relaxation in the conduction band of a QD ensemble. **a** In two out of five identical QDs, the lower confined state is populated, corresponding to a probability of $f = 0.4$, so that the relaxation of a second carrier from the upper confined state is blocked. At the same time, in the remaining three dots the relaxation is possible. In the Boltzmann description of the ensemble **(b)** the relaxation rate is weakened by a factor $(1 - f)$, which describes the average availability of the final state, indicated by a single QD with a "ghost" carrier present in the lower state

character of the vNL equation. In contrast, the nonlinear Boltzmann equation yields a power law behaviour, which is significantly slower than the exponential convergence and which can not be assigned a constant rate. In the regime of high excitation, where a large number of relaxation channels is available, carrier correlations are destroyed on a short time scale and a mean-field description of scattering becomes feasible again.

After these general considerations, we discuss the two relevant types of system-reservoir coupling, namely carrier-carrier Coulomb scattering and carrier scattering by phonons. First, the contact of the QD carriers with the carriers in delocalized states leads to various Auger-like scattering processes. These are beyond the interaction of QD carriers among each other, which is already taken care of in the system Hamiltonian H_S. Carriers are captured or ejected from the QD and they scatter between localized states due to the Coulomb interaction with delocalized carriers; the latter provide the necessary energy for the transition processes. A detailed analysis of these processes and the corresponding rates have been given in [9].

A second type of reservoir is provided by the phonons in the barrier material. In polar semiconductors one of the strongest contribution to carrier scattering processes is due to LO phonons, for which we assume a dispersionless spectrum $\omega_{\boldsymbol{q}} = \omega_{LO}$. The interaction between QD system and phonon reservoir is described by the Hamiltonian

$$H_{SR} = \sum_{i,j,\boldsymbol{q}} M_{\boldsymbol{q}}^{i,j} a_i^\dagger a_j \left(D_{\boldsymbol{q}} + D_{-\boldsymbol{q}}^\dagger\right), \tag{1.11}$$

with the Fröhlich coupling matrix elements $M_{\boldsymbol{q}}^{i,j}$ [78]. In (1.11) two scenarios can be distinguished. First, when both indices i, j refer to QD states, electronic transitions $|j\rangle \rightarrow |i\rangle$ inside the QD assisted by the emission or absorption of phonons are described, leading to carrier relaxation in the QD. The second case involves a QD and a delocalized state and corresponds to carrier capture from or reemission

into the reservoir, again assisted by phonons. For the first case, treating all possible transitions X between configurations, which include the movement of a carrier from $|j\rangle$ to $|i\rangle$, one obtains in Born-Markov approximation the transition rate in the form

$$\gamma_X = \frac{2\pi}{\hbar^2} \sum_{\boldsymbol{q}} |M_{\boldsymbol{q}}^{i,j}|^2 \left\{ (1 + N_{LO})\, \delta(\omega_X + \omega_{LO}) + N_{LO}\, \delta(\omega_X - \omega_{LO}) \right\}. \quad (1.12)$$

N_{LO} is the phonon population at the lattice temperature. The first term corresponds to processes involving phonon emission, the second involving phonon absorption. In (1.12) one encounters a problem that is specific to the LO-phonon driven carrier kinetics in discrete electronic systems. The strict energy conservation expressed by the δ-functions is not generally met. In early theoretical considerations [79, 80], this observation has lead to the prediction of a "phonon bottleneck". However, only in lowest-order perturbation theory (Fermi's golden rule) does the scattering rate vanish. Equation (1.12) corresponds to this level, which results from applying the Born-Markov approximation. A better-suited non-perturbative description leads to the polaron picture. The quasiparticle renormalization effects of the non-perturbative treatment can be included in a generalized form of (1.12) via spectral functions combining the configuration picture with the formalism of many-particle Green's functions, as described in detail in [56]. In contrast to the phonon bottleneck predicted from perturbation theory, non-vanishing scattering rates are obtained from this approach. The Green's function formalism allows for a self-consistent treatment of carrier-carrier and carrier-phonon interaction, leading to a non-trivial co-action of both mechanisms and modifying all transition rates entering the vNL equation.

In [56], we use the theory introduced above to analyze experimental results for the carrier capture and relaxation dynamics in self-organized semiconductor QDs, which are obtained by time-resolved differential transmission (TRDT) measurements. Figure 1.10 contains examples of TRDT traces for the ground-state transition at different temperatures and fixed excitation power. From the TRDT signals, rise times can be extracted that reflect the efficiency of carrier capture and relaxation processes under different experimental conditions. The data can be understood from simulations of TRDT rise times under comparable conditions taking into account both carrier-carrier and carrier-phonon interaction. The results are collected in Fig. 1.11. In agreement with the experiment, we find a higher temperature sensitivity at lower carrier densities, which points to a dominant role of the phonon scattering in this regime. For low temperatures, the transition rate increases strongly with the carrier density due to more efficient carrier-carrier scattering (Auger-like processes assisted by delocalized carriers). The latter also causes larger broadening of the spectral functions, which in turn accelerates carrier-phonon scattering as well. For elevated temperatures, the density dependence is weak due to a dominating phonon contribution. As shown in [56], renormalization effects are of critical importance for this agreement, which can not be achieved by a perturbative treatment of system-reservoir interaction.

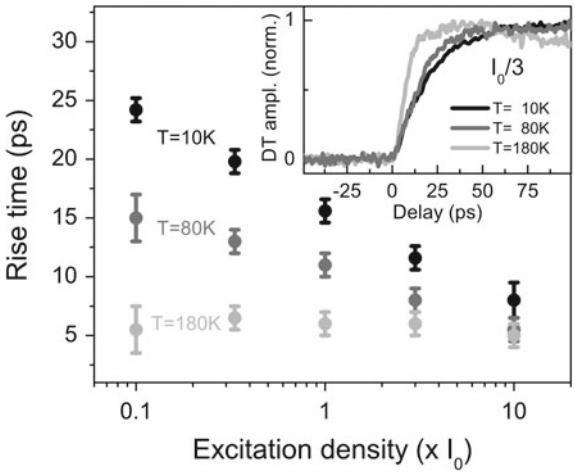

Fig. 1.10 Rise times extracted from monoexponential fits to time-resolved differential transmission (TRDT) transients of the QD ground state, obtained at various excitation intensities for temperatures T = 10, 80, and 180 K. The inset shows DT traces at an excitation density of $I_0/3$ with $I_0 = 40\,\mathrm{W/cm^2}$

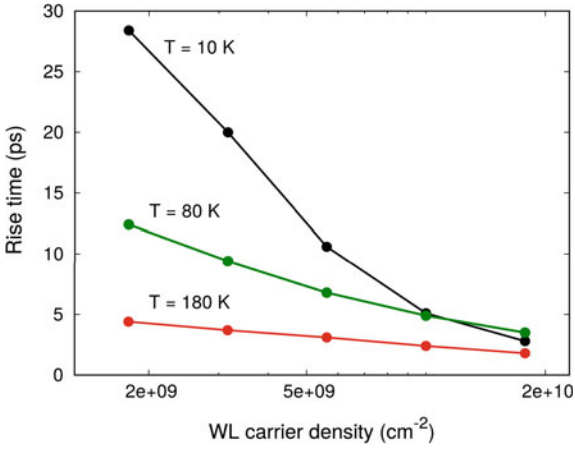

Fig. 1.11 Rise time of the TRDT signal for the QD ground state calculated as a function of the wetting-layer (WL) carrier density for different temperatures. Both carrier-carrier and carrier-phonon interaction are considered within a non-perturbative theory including joint quasiparticle renormalizations in the multi-exciton configuration-picture description

The many-particle interaction of the QD system with its environment induces not only transitions between QD configurations, but also dephasing of coherences in the QD that may be generated by resonant optical excitation. In the vNL equation (1.10), this is reflected by a decay of transition amplitudes between many-particle configurations. As widely discussed in the following chapters of this book, the amount of dephasing is crucial for quantum optical and quantum information applications of QD emitters, as it is directly connected to broadening of emission lines and to the lifetime of coherences that are exploited for the generation of entanglement. For example, dephasing affects the deterministic creation of photons by limiting the fidelity of resonant excitation of single QD transitions which is discussed in the chapters by *Rengstl*, *Jetter* and *Michler* and by *Portalupi* and *Michler*. This problem also appears in the context of spin preparation by optical pulses, which is the topic of the chapter by *Sun* and *Waks*. The limitation of indistinguishability of

entangled photons due to dephasing is addressed in the chapters by *Weihs*, *Huber* and *Predojević* and by *Heindel*, *Rodt* and *Reitzenstein* while *Brash*, *Liu* and *Fox* very nicely express how strongly coherent control experiments in semiconductors rely on a reduction of dephasing for example due to carrier-phonon and carrier-carrier scattering.

In [5], the dephasing due to carrier-carrier and carrier-LO-phonon interaction in semiconductor QDs has been quantified focussing on the regime of elevated excitation density. Complementary to this is the low-density regime, where acoustic phonons and especially at low temperature Coulomb-mediated out-scattering of QD carriers lead to homogeneous broadening, see the contribution of P. Borri and W. Langbein in [23]. The pure dephasing associated with acoustic phonons can be comparable to scattering-induced dephasing when the carrier density is low. The homogeneous exciton linewidth has been studied in great detail experimentally [61, 81, 82] and theoretically using the independent Boson model, where the electronic system is described in a two-level approach [83–87]. Fewer experiments have investigated the dephasing of many-particle configurations [88–90].

1.4 Non-resonant QD-cavity Coupling

For weak excitation of self-assembled semiconductor QDs, the ground-state exciton is dominating, while at elevated excitation levels a rich structure of closely lying discrete optical transitions can be observed [63]. When QDs are placed in a high-Q microcavity, the narrow-linewidth mode singles out particular transitions. In contrast to atom-like isolated emitters, QDs exhibit an interesting peculiarity: Even for weak excitation and QD emission lines significantly detuned from the cavity resonance, photons can be emitted into the cavity mode. As a result of extensive experimental and theoretical investigations, different mechanisms are discussed in the literature. These involve phonon-assisted optical processes, non-resonant coupling mediated by multi-exciton transitions, and Coulomb-assisted non-resonant coupling.

The effect is mostly discussed in the context of individual QDs coupled to optical cavities. Beyond this, in cavity-QED lasers non-resonant QD-cavity coupling is also expected to be responsible for a frequently observed background emission contribution. In these cavity-QED lasers the number of resonant QD emitters is often too small to reach stimulated emission, which is nonetheless observed in corresponding experiments [8, 46, 91, 92].

1.4.1 Phonon-Assisted Non-resonant Coupling

The acoustic phonons have been connected [85, 86, 93] with a particular line shape of the excitonic transition. The dominant contribution to the carrier-phonon coupling is contained in the diagonal matrix elements with respect to the carrier-state index,

which facilitates the application of the independent boson model [78]. The role of LA-phonons in the off-resonant cavity feeding was demonstrated [94–101]. It was shown [2, 102–104] that the appropriate frame work to describe the phonon-assisted energy transfer between the exciton and the cavity is provided by the polaron picture, in which the exciton generates an electric field to which the lattice ions react by displacements of their oscillation centers. A polaron transform can be used to connect the distorted lattice with the original one, and the QD-phonon interaction can be formally eliminated from the Hamiltonian [78]. As a result the Jaynes–Cummings Hamiltonian

$$\tilde{H}_{JC} = g\,(b^\dagger X\, B^\dagger + b\, X^\dagger\, B) \tag{1.13}$$

then includes phonon operators

$$B = \exp\left[\frac{M_q}{\omega_q}(D^\dagger_{-\mathbf{q}} - D_{\mathbf{q}})\right] \tag{1.14}$$

besides the usual carrier ($X = a_i^\dagger a_j$) and photon ones. The relevant coupling constant in the problem is the difference between those of the conduction and valance band states, $M_q = M_q^{i,i} - M_q^{j,j}$. With the phonons acting as a thermal bath, a system-reservoir treatment leads to Lindblad terms $\mathscr{L}_{b^\dagger X}$ and $\mathscr{L}_{bX^\dagger}$. In this case, the associated off-resonant cavity feeding rates as a function of detuning read

$$\gamma_{b^\dagger X}(\Delta) = 2g^2\,\langle B\rangle^2\,\mathrm{Re}\int_0^\infty \mathrm{d}t\; e^{-i\Delta t}(e^{\Phi(t)} - 1)\;, \tag{1.15}$$

with $\Phi(t)$ given by

$$\Phi(t) = \sum_q \left|\frac{M_q}{\omega_q}\right|^2 \left[(N_q + 1)e^{-i\omega_q t} + N_q e^{i\omega_q t}\right]\;. \tag{1.16}$$

The rate of the reverse transition is related to the above one by the thermal factor $e^{-\beta\Delta}$, as prescribed by the Kubo-Martin-Schwinger condition. When expanding the Φ exponential in (1.15), all multi-phonon processes of emission and absorption that generate a total energy of Δ can be seen to contribute. A more detailed discussion of this polaron master equation approach is given in the chapter of *Roy-Choudhury* and *Hughes*.

In Fig. 1.12 the phonon-assisted cavity-feeding rate is shown for typical InGaAs QD parameters [4]. There is a pronounced asymmetry between positive and negative detuning for low temperature. This is expected, since any thermal bath favors the process which lowers the system energy, all the more so at low temperatures. For a lattice temperature of 20 K efficient cavity feeding is obtained only up to detunings

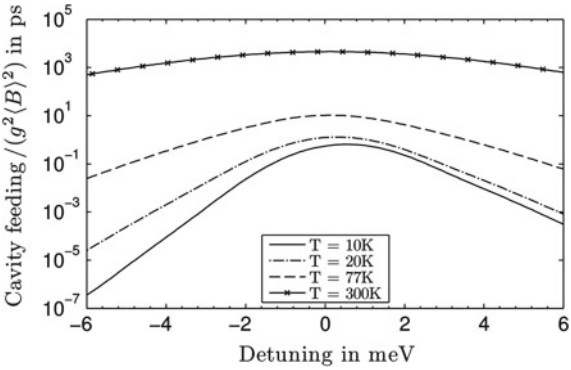

Fig. 1.12 Effective cavity feeding rates due to the QD-phonon coupling as a function of the detuning from the cavity resonance. Results are calculated from (1.15) and shown for 10, 20, 77 and 300 K

∼2 meV between the transition and the mode. Nevertheless, we find that phonon-assisted recombination of QD excitations within this detuning range can lead to an emission enhancement in a cavity QED laser that can make the difference between thermal or coherent emission [4].

Many quantum optical application require state preparation with high fidelity. Phonon-assisted processes can be utilized to efficiently prepare e.g. the biexciton or exciton state by tuning the optical excitation on the corresponding phonon-sidebands as discussed in the chapters of *Portalupi* and *Michler* as well as *Roy-Choudhury* and *Hughes*.

1.4.2 Non-resonant Coupling Mediated by Multi-exciton Transitions

A quantification of cavity feeding effects is typically hindered in systems with many emitters. Here, various emission channels of different emitters overlap, masking individual emission properties. The few-emitter limit on the other hand offers the unique possibility to study non-resonant mode coupling in a highly controllable environment. Photonic crystal (PhC) [105] cavities in particular provide strong optical confinement with high Q factor and small mode volume [106], making them suitable to explore the miniaturization limit of lasing where the gain medium consists only of a few solid-state quantum emitters within a single mode cavity [91, 107].

Figure 1.13a shows the cavity-mode emission of a few (N ∼ 4) QDs located in a PhC nanocavity. The QD ground-state exciton to cavity detuning is much larger than 2 meV. At first it may seem contradictory that lasing can be achieved in such a system. However, the discrete QD lines in Fig. 1.13a evolve into a broadband emission at elevated excitation intensities (highlighted by the gray shaded region). This is due to non-resonant coupling facilitated by a multitude of closely spaced excited multi-exciton states, some of which are overlapping with the cavity mode. More precisely, when a QD can accommodate many single-particle bound states, the number of

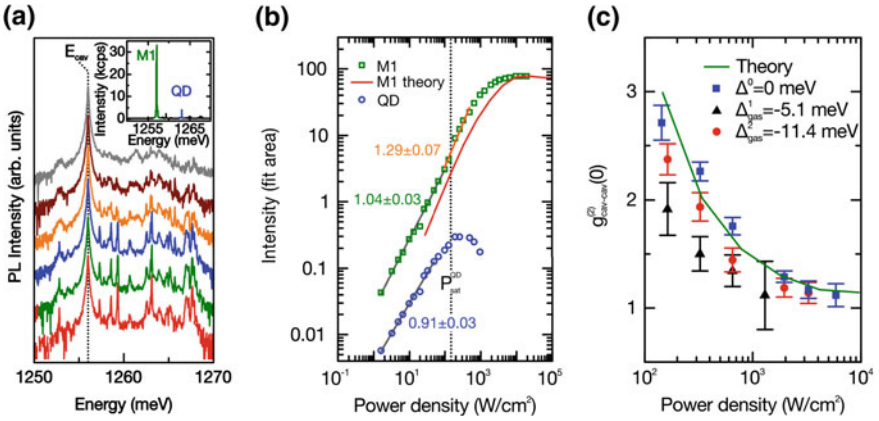

Fig. 1.13 **a** Experimental results for the emission spectrum from the cavity and increasing cw excitation power density. The spectra are plotted on a logarithmic scale with an offset to each other for clarity. The cavity mode is labeled E_{cav}. The inset shows a linear spectrum of the system for an excitation power density of $P_{\mathrm{sat}}^{\mathrm{QD}}$. **b** Integrated intensity of the cavity mode (*green*) and the QD (*blue*) as a function of excitation power density. *Black solid lines* represent power-law fits to the emission data. The *solid red line* depicts the intensity of the cavity mode emission calculated from theory. To connect the theoretical pump rate with the experimental power density, the *red curve* has been shifted along the power axis to ensure that the calculated exciton saturation coincides with $P_{\mathrm{sat}}^{\mathrm{QD}}$. **c** Second oder correlation $g^{(2)}(0)$ as function of the excitation power density. The colors represent three different cavity mode energies. The *solid green line* has been obtained from the microscopic model (color figure online)

carrier configurations becomes quite large, and their Coulomb interaction results in many closely spaced multiexcitonic transitions. When a QD is excited with multiple carriers, the subsequent relaxation dynamics of the carriers into a quasi-equilibrium state usually involves transitions between multiple configurations, and due to the Coulomb-configuration interaction, these configurations are associated with largely varying multi-exciton energies, which are then passed through the relaxation process. As soon as one of these configuration energies overlaps with the cavity mode, a Purcell-enhanced photon emission [63, 108, 109] can take place at larger detunings from the ground-state exciton. It is due to these transitions that lasing is possible even if the discrete ground-state excitons of the four QDs visible in the lower spectra in Fig. 1.13a are detuned from the mode by up to 17 meV.

The input-output characteristics at the cavity energy shows a slight superlinear increase for excitation-power densities and appears simultaneously with the saturation of the QD ground-state exciton, when multi-exciton states become increasingly populated with significant probability, see Fig. 1.13b. For all detunings between emitter transitions and mode, a clear transition from the spontaneous-emission regime with $g^{(2)}(0) > 1$ to coherent lasing with $g^{(2)}(0) = 1$ is observed with increasing excitation-power density, see Fig. 1.13c. Thus, in this example, the absolute energies

of QD-transitions and cavity mode are of limited importance for the operation of the nanolaser.

To study the interplay of QD many-particle states and the resulting coupling to the cavity mode, we have solved the von Neumann-Lindblad equation for the system of four QDs and the quantized field of the cavity. Due to the large state space, calculations can only be performed for a subset of the QD many-particle configurations. When one of the excited configurations is in resonance with the cavity mode, we obtain results for the mean photon number similar to the experiment. Moreover, it turns out that in order to simultaneously describe the experimental results for intensity and $g^{(2)}(0)$, we need to assume that two of the excited configurations are resonant with the cavity mode. When performing independent configuration-interaction calculations for multi-exciton states, even for small QDs with a limited number of single-particle states, we find a very large number of excited multi-exciton states with largely varying configuration energies corresponding, e.g., to two or three electron-hole pairs (3X and 2X). Hence we assume that from each of the transitions within the manifold $3X^* \rightarrow 2X^*$ and $2X^* \rightarrow 1X^*$, one is resonant with the cavity mode. Here X^* represents an excited exciton state.

The theoretical results for the mean photon number and photon autocorrelation function are added as solid lines in Fig. 1.13b, c. Interestingly, in the low-excitation regime values up to $g^{(2)}(0) = 2.7$ are observed. From the theoretical model, we can attribute this enhanced probability of two- and multiple-photon emission events to two effects: One is the presence of competing resonant emission channels for each QD emitter, allowing for the simultaneous emission of photons into the mode. The second results from strong radiative coupling between different emitters associated with the effect of superradiance. This effect has been predicted in [110, 111] for QD nanolasers under continuous-wave excitation, and experimental proof in a system under pulsed excitation will be discussed in Sect. 1.5.

1.4.3 Coulomb-Assisted Non-resonant Coupling

In addition to the contributions from multi-exciton states, the role of the interaction with the delocalized states was recognized [109] and Coulomb hybridization of QD bound states with the delocalized states was demonstrated [112, 113]. In fact, carriers in the delocalized states can act as a thermal bath, which is able to compensate for the energy mismatch between a QD transition and the cavity resonance via Auger-like processes. This is an alternative mechanism to the Coulomb configuration interaction between carriers [109], as the Coulomb interaction involves other carriers outside of the QD. Importantly, its effect in opening a kinetic channel is present even for QDs hosting very few confined states, and holds even for a QD with single electron and hole levels.

To describe this mechanism, we start from the Hamiltonian containing the Jaynes–Cummings (JC) part for the interaction of the QD exciton with photons of the cavity mode as well as the Coulomb part for the interaction between QD and

delocalized states. Two different techniques can be used to formally eliminate either (i) the exciton-photon or (ii) the Coulomb interaction part from the Hamiltonian. Specifically, in (i) the Schrieffer-Wolff transformation [78, 102] can be used that amounts to a perturbative diagonalization of the JC interaction part. The delocalized states remain unchanged, and the Coulomb interaction is felt by the photon subsystem due to the dressing of the QD states with the JC interaction.

A second approach considers a different scenario, in which the carrier-bath interaction is partly diagonalized and was used in Sect. 1.4.1 for the treatment of the phonon-assisted coupling. In [114] we extend the procedure to the case of the fermionic bath of carriers in delocalized states. The model is not exactly soluble but can be handled diagrammatically. The major difference to the first approach is that now the bath adapts itself to the presence or absence of the exciton.

A qualitative discussion can already be obtained within the Schrieffer-Wolff approach (SWA). Using this formalism, we obtain an effective JC interaction Hamiltonian

$$H'_{\mathrm{int,SWA}} = -\frac{g}{\Delta}\, W\, (b^\dagger\, X + b\, X^\dagger) \tag{1.17}$$

that describes transitions between the QD exciton and the cavity photons, assisted by the Coulomb interaction with carriers in delocalized states. We consider the fermionic reservoir as being stationary and in thermal equilibrium and obtain Lindblad terms, $\mathscr{L}_{b^\dagger X}$ and $\mathscr{L}_{b\,X^\dagger}$, with rates given by

$$\gamma_{b^\dagger X} = 2\pi \frac{g^2}{\Delta^2} \sum_{\lambda,\mathbf{k},\mathbf{k}'} \left|W^\lambda_{\mathbf{k},\mathbf{k}'}\right|^2 f^\lambda_{\mathbf{k}}(1 - f^\lambda_{\mathbf{k}'})\, \delta(\Delta + \varepsilon^\lambda_{\mathbf{k}} - \varepsilon^\lambda_{\mathbf{k}'})\,. \tag{1.18}$$

Here, the occupancies $f^\lambda_{\mathbf{k}}$ are Fermi functions describing the carrier population of electrons and holes ($\lambda = e, h$) in the delocalized states. Similarly, $\gamma_{b\,X^\dagger}$ follows by changing Δ to $-\Delta$. In Fig. 1.14 we show results for the Coulomb-assisted feeding rate as a function of detuning. With increasing density n of carriers in delocalized states additional scattering channels can compensate for the energetic mismatch Δ between exciton and cavity, which leads to an increasing feeding rate. For comparison, we show the spontaneous emission rate caused by the JC coupling alone for typical QD-cavity parameter. At low carrier density, Coulomb assisted cavity feeding is negligible in comparison to the spontaneous emission rate, which is in agreement with previous experiments performed under low excitation condition [94, 97], in which only phonon signatures were found. However, for sufficiently high carrier densities ($n > 10^{10}/\mathrm{cm}^2$) Coulomb assisted processes prevail even at large detuning and lead to a significant cavity feeding that is one order of magnitude stronger in comparison to the JC coupling alone.

Finally, we find a significant reduction of the off-resonant cavity feeding, if the wave functions for electrons and holes are similar (lines without dots). The reason is a large degree of compensation between the electrostatic (Hartree) Coulomb integrals contributing to (1.18). For identical electron and hole wave functions, the exciton

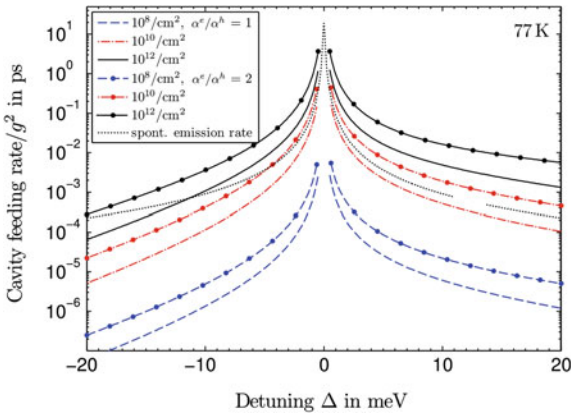

Fig. 1.14 Cavity-feeding rate for a non-resonant QD coupled to the continuum of delocalized states at a temperature of 77 K obtained by using the SWA. We vary the carrier density in the delocalized states n from 10^8–$10^{12}/\mathrm{cm}^2$ and consider electron and hole envelopes that are equal (*lines without dots*) or differ by a factor of two (*lines with dots*). In all calculations we use InGaAs parameters [9] and assume flat lens-shaped QDs. For comparison the spontaneous emission rate is shown (*dotted line*) for typical parameters ($\kappa = 0.1/\mathrm{ps}$, $\Gamma = 0.01/\mathrm{ps}$, $P = 0.1/\mathrm{ps}$). Note that the rates are normalized to the square of the light-matter coupling strength

is not only globally but also *locally* neutral and there is no electrostatic interaction between the exciton and the carriers in the delocalized states. Classically, the system and the bath become uncoupled, only the exchange interaction is left. This points to an intrinsic difference between interband cavity assisted feeding and intraband scattering processes: In the latter case, electrons and holes can scatter independently, while in the former case the emission of a photon requires the presence of an exciton, i.e., a fully correlated electron-hole pair. As a consequence, any formalism describing the off-resonant cavity feeding, which relies on an interaction of Coulombian origin, like Auger interaction between the QD and carriers in delocalized states, or Fröhlich interaction of QD carriers with LO phonons, must obey a local neutrality condition: for locally neutral excitons and discarding the exchange terms the off-resonant process should vanish exactly.

1.5 Superradiant Emitter Coupling of Quantum Dots in Optical Resonators

In a conventional laser, the below-threshold spontaneous emission stems from independent emitters while the above-threshold stimulated emission – within a classical picture – results from a phase synchronization of the emitters with the radiation field. In terms of a quantum mechanical picture, the de-excitation of the active material, in semiconductors due to the recombination of electron-hole-pairs, is linked to

photon generation in a way, that the expectation value $\langle b^\dagger \sigma_i^- \rangle$ has a finite value. Here $\sigma_i^- = v_i^\dagger c_i$ represents a microscopic polarization due to the de-excitation of the emitter i. $v_i^\dagger$ denotes a creation operator for a valence electron and c_i an annihilation operator for a conduction electron in the i-th QD. For independent emitters, the total emission rate is simply the sum of contributions from independent emitters, and quantum mechanical correlations are absent between the microscopic polarizations of different emitters. This is the typical situation for the above-threshold emission of conventional lasers. The phenomenon of radiative emitter coupling leads to the existence of correlations of the form $\langle \sigma_j^+ \sigma_i^- \rangle$ between the polarizations of different emitters i and j. The emitter i looses an excitation at the cost of adding an excitation in emitter j without changing the photon number in the system. Such a correlation can be driven by the exchange of a photon between the emitters. It leads to the phenomenon of superradiance, for which the emission rate of the ensemble can be enhanced or inhibited in comparison to independent emitters. For the latter effect, the term "subradiant emission regime" is also used.

Since the prediction of superradiance by Dicke in 1954, the effect has been extensively studied in a variety of systems [115, 116] including semiconductor QDs [117, 118]. In most cases the demonstration of superradiance relies on macroscopic emission properties, where the time-resolved intensity or emission linewidth changes in comparison to individual emitters. Most prominent is the transition from the exponential decay of independent emitters to a superradiant pulse for correlated emitters [115], even though most experiments resort to decay-time changes as function of the emitter number. The recent interest in superradiance of superconducting qubits [119], trapped atoms [120], and semiconductor magneto-plasmas [121] was motivated by the prospects to study directly the correlated state of the active material.

In this chapter, we demonstrate the influence of radiative emitter coupling, which leads to electronic correlations among different emitters, on the emission properties of QDs in optical resonators. We find a clear influence on the time-resolved emission (the occurrence of a superradiant pulse) as well as on the emission intensity. Especially at low excitation, dipole anti-correlations between pairs of emitters lead to "excitation trapping" in the so-called subradiant regime. As a consequence, we identify modified characteristic properties of nanolasers that exhibit radiative coupling effects, such as a non-constant β factor that reduces strongly in the low-excitation regime. Furthermore, electronic correlations have a direct influence on the statistical properties of the emitted photons. The effect of super-bunching has been predicted in [122, 123] and was recently demonstrated in direct comparison between theory and experiment in [6, 124].

In this section we consider cavity-QED lasers that operate with self-organized semiconductor QDs within a resonator acting as gain material. The QDs are excited by optical pumping and for the subsequent emission, the time-resolved and time-integrated intensity are analyzed. To characterize the statistical properties of the emission, the second-order photon correlation function $g^{(2)}(\tau = 0)$ is used (cf. Sect. 1.1.2). For the latter, a comparison of different emission regimes is presented in Fig. 1.15. In particular, a value of $g^{(2)} > 2$ is indicative for radiative coupling (case

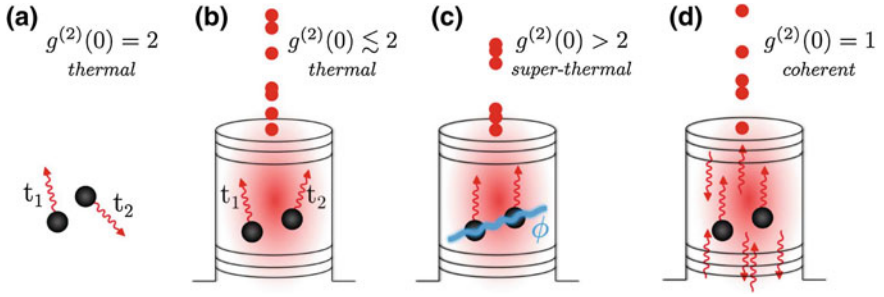

Fig. 1.15 Illustration of emission regimes. **a** Spontaneous recombination from independent emitters leads to thermal radiation. **b** Using three-dimensional photon confinement in a cavity-quantum electrodynamics laser, spontaneous emission is directed into a single resonator mode. For independent emitters, below threshold the photon emission is uncorrelated, producing thermal or close to thermal light. **c** The exchange of photons introduces correlations between the electronic states of different emitters. A relative phase information ϕ is spontaneously established, and the emission from this entangled many-particle state leads to a superradiant pulse with giant photon bunching. **d** Above threshold, stimulated emission dominates and leads to coherent radiation

c) between distant emitters [110, 122, 123]. In atomic systems, inhomogeneous distributions of the emitter energies and light-matter couplings have a strong detrimental effect on the radiative emitter coupling. For self-organized semiconductor QDs, the role of inhomogeneous broadening is substantially mitigated by the effect of non-resonant QD-cavity coupling discussed in the previous paragraph. It involves the ability to efficiently couple slightly detuned QDs to the cavity mode. Hence the cavity serves a two-fold purpose. It provides a channel for efficient photon exchange between emitters, which drives the inter-emitter correlations, and it enhances the coupling of slightly off-resonant emitters.

For the theoretical description of such a system, two options are available. When considering a small number of emitters, typically less than 10, a direct numerical solution of the von Neumann-Lindblad equation can be used [4–6, 122, 123]. This method has the advantage, that the full quantum dynamics of the coupled emitters and cavity-field system can be described. As a result, the density matrix of this system is available. It includes all existing quantum correlations and facilitates the calculation of various correlation functions. The drawback is, that only a small number of emitters can be included and each emitter is often only represented by a two-level system [122, 123, 125] or with few electronic configurations [4–6], since otherwise the Hilbert space (and the resulting dimension of the density matrix) becomes too large for a direct numerical solution. To describe larger systems, such as QD-ensemble lasers consisting of hundreds of emitters, the equation-of-motion technique can be used. By means of the cluster-expansion technique, a closed set of equations can be derived to include quantum correlations up to a given order, see Sect. 1.1.1. In [110, 124], a closed set of equations has been derived that contains inter-emitter correlations of the type $\langle \sigma_j^+ \sigma_i^- \rangle$, and the resulting changes in the cavity photon number $\langle b^\dagger b \rangle$ and in the second-order photon correlation function $g^{(2)}(\tau = 0)$.

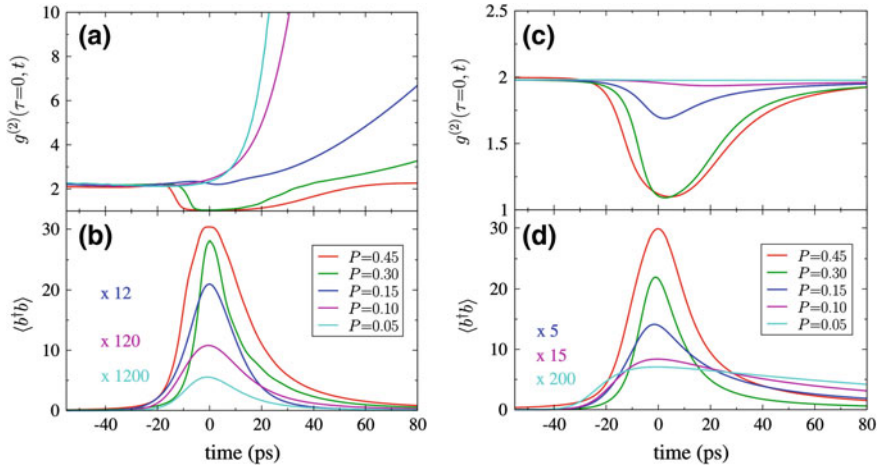

Fig. 1.16 Time evolution of the intensity autocorrelation function $g^{(2)}(\tau = 0, t)$ (*top*) and mean photon number (*bottom*) after pulsed excitation of a nanolaser with various pump-pulse areas P. *Different curves* correspond to below-threshold excitation ($P = 0.05$), the transition region ($P = 0.1$ and 0.15), and above-threshold excitation ($P = 0.3$ and 0.45). In the *left part*, superradiant coupling between different quantum dots is included, while in the *right part* it is omitted

Figures 1.16 and 1.17 show results of such a theory for a QD nanolaser working with 200 QD emitters within an optical resonator (cavity photon decay rate $\kappa = 0.4\,\mathrm{ps}^{-1}$, coupling rate between QDs and cavity mode $g = 0.1\,\mathrm{ps}^{-1}$, spontaneous emission rate into other modes $\gamma_{nl} = 0.005\,\mathrm{ps}^{-1}$). In Fig. 1.16, the time evolution of the mean photon number and second-order photon correlation function are compared with (left part) and without (right part) superradiant coupling. In the presence of superradiant coupling, even for weak pump rates a short output pulse is obtained with a temporal width of about 20 ps, which is much shorter than the spontaneous lifetime of individual emitters in the cavity (about 200 ps). At the same time, $g^{(2)}(\tau = 0, t)$ is about 2 during the pulse maximum, indicating that the short pulse width is not linked to stimulated emission. Values for $g^{(2)}(\tau = 0, t)$ larger than 2 before and in particular after the pulse maximum are signatures of radiative emitter coupling. When omitting the radiative emitter coupling in the theory, $g^{(2)}(\tau = 0, t)$ remains 2 for weak pumping and the time-resolved emission shows a much slower exponential decay with the typical Purcell-enhanced lifetime of individual emitters (see also the left panel in Fig. 1.17). For stronger pump pulses, the system is driven above the laser threshold and a stimulated emission pulse can be identified with $g^{(2)}(\tau = 0, t)$ reaching a value of 1 during the pulse maximum. In this regime, the difference in the theoretical results with and without radiative emitter coupling becomes small, which indicates that stimulated emission dominates the photon generation and suppresses the role of inter-emitter correlations.

For the pulsed optical excitation discussed in the above examples, the time-integrated output intensity versus pump pulse area is shown in the right part of

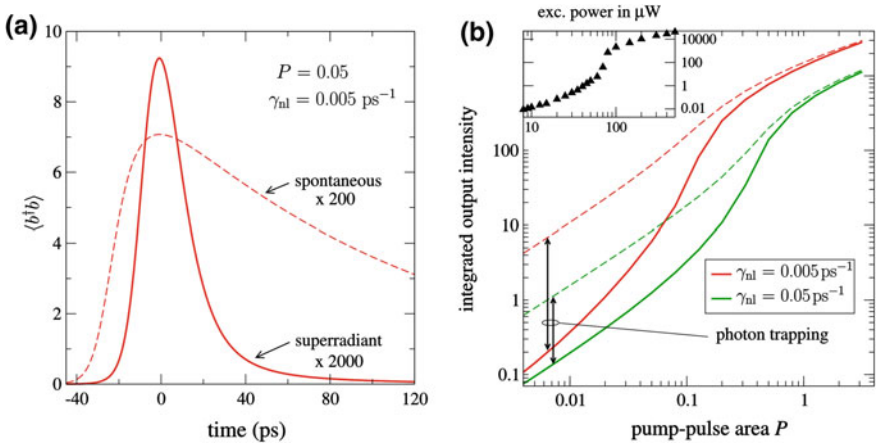

Fig. 1.17 Calculated time evolution of the cavity mean photon number after pulsed optical excitation for weak pumping (*left*) and time integrated output intensity versus pump-pulse area (*right*). Results including superradiant coupling of the emitters (*solid lines*) are compared to those for independent emitters (*dashed lines*). As indicated in the *right panel*, a stronger spontaneous emission rate into non-lasing modes γ_{nl} decreases the threshold modification due to superradiant coupling but corroborates the robustness of the effect. The inset confirms the presence of the threshold kink in the experiment despite a large β-factor as an indication of excitation trapping due to superradiant emitter coupling

Fig. 1.17. When comparing results with (solid lines) and without (dashed lines) superradiant coupling, a dramatic reduction of the output intensity for weak and intermediate pump rates is evident. In this regime, photons emitted into the cavity mode from the QDs are reabsorbed by other QDs in a way that inter-QD polarizations of the form $\langle \sigma_j^+ \sigma_i^- \rangle$ are driven. These inter-QD polarizations exist in addition to the photon-assisted polarization $\langle b^\dagger \sigma_i^- \rangle$. The build-up of the former clearly reduces the photon number in the cavity mode. On the other hand, above the laser threshold, when stimulated emission is present, the role of radiative emitter coupling is small. The combination of these two observations leads to a larger jump in the input-output curve at the laser threshold [110, 124]. In the standard rate-equation laser theory, this jump is solely determined by the β factor [126], which quantifies the fraction of the total spontaneous emission that is directed into the laser mode. From a rate-equation model it is found that β is solely determined by the relation of the rates associated with emission into the laser mode γ_l and into non-lasing modes or other loss channels γ_{nl}, i.e., $\beta = \gamma_l/(\gamma_l + \gamma_{nl})$ [127]. Correspondingly, for cavity-QED lasers the β factor is frequently estimated from the jump in the input-output curve. Our results demonstrate that in the presence of radiative coupling this strongly underestimates the value for β. Furthermore, without superradiant coupling a larger γ_{nl} leads to a larger kink as the β factor increases. Our calculation including radiative coupling leads to a smaller kink, as a larger γ_{nl} causes a reduction (damping) of inter-QD polarizations, thereby reducing the associated excitation trapping (right panel of Fig. 1.17).

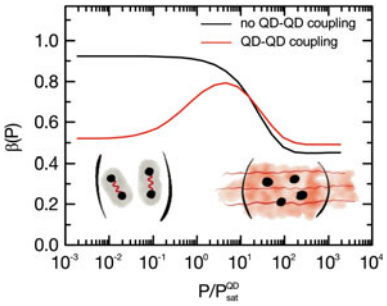

Fig. 1.18 (*Red curve*) pump-rate dependent β-factor obtained from the theoretical model with parameters applicable to experimentally studied system. (*Black curve*) calculation suppressing radiative coupling effects between emitters that are responsible for sub- and superradiant effects. Comparing *both curves* reveals that radiative coupling effects lead to a strong inhibition of spontaneous emission at low excitation (subradiance) and a slight enhancement of spontaneous emission above the laser threshold (superradiance)

This behavior actually raises the question whether a constant β factor is suited to characterize QD nanolasers that, due to the strong mode confinement, are likely to facilitate the formation of inter-emitter correlations by the light field. In the following, we suggest the idea of introducing a pump-rate dependent factor $\beta(P)$ that accounts for a reduction of the spontaneous emission rate due to excitation trapping, as well as for the interplay of different multi-exciton configurations and apply it to the few-QD nanolaser system discussed in the context of Fig. 1.13.

We first discuss the result for the pump-rate dependent $\beta(P)$ factor without the effects of radiative coupling, shown by the black curve in Fig. 1.18. The asymptotic values at low ($\beta(P) > 90\%$) and high excitation ($\beta(P) \approx 50\%$) reflect the conventional constant β factor associated with the multi-exciton transitions that dominate at low and high excitation. In between, a transition is seen as the system switches between multi-excitonic emission channels from different manifolds, cf. Sect. 1.4.2. To provide insight into the role of the radiative coupling in our system, the red curve shows the pump-rate dependent $\beta(P)$ factor calculated including correlations due to radiative coupling. In the low-excitation regime, where the super-thermal bunching is observed in $g^{(2)}(0)$ (Fig. 1.13c), inter-emitter coupling leads to a strong inhibition of the spontaneous emission rate resulting in $\beta(P) = 50\%$ instead of 90%. Thereby $\beta(P)$ reflects the photon-trapping effect discussed above.

In summary, radiative emitter coupling can influence classical emission properties like the intensity and its temporal evolution, but also the statistical properties of the light emission. The effects of inter-emitter coupling is most prominent in the spontaneous emission regime, but can also play a role in few-emitter lasers, where stimulated emission is weak. Accounting for radiative coupling effects in cavity-QED lasers can strongly modify the device characteristics and be of paramount importance for the correct identification of system parameters, opening up new research directions in cavity-QED nanolasers.

1.6 Summary and Outlook

Advances in the quantum information technologies have created a demand for fast, efficient, and integrable sources of non-classical light. Solid-state emitters are a promising platform, and quantum-dot systems have reached a technological maturity that permits a high level of control over their emission properties, beginning by tailoring the emission wavelength via material and growth design, but also altering spontaneous emission itself by using cavity-QED effects in microcavities. As a result, nearly many imaginable states of the light field can be realized with single or few-QD systems, from single-photon Fock-states to intense highly-bunched super-thermal light.

Theoretical models play an important role in the design of new devices, the definition of achievable specifications, and the exploration of new applications not yet thought of. Unlike atomic systems, QDs are not isolated but are embedded semiconductor systems. Theoretical modelling must combine quantum-optics with semiconductor physics. This chapter has given an overview over the constituents of such a theory and possible methods using examples from different applications.

The sophistication of technological possibilities will lead to even more advanced realizations of solid-state cavity-QED systems in the future. New materials such as two-dimensional semiconductors based on transition-metal dichalcogenides hold great promise for exploring excitonic effects up to room temperature. Individual cavities can already be combined to cavity arrays, so-called Jaynes–Cummings lattices, in which many-body systems such as the Bose–Hubbard model become realized. The potential of such systems for the quantum-information technologies is largely unexplored.

Acknowledgements The authors would like to thank Weng W. Chow (Albuquerque), Jan Wiersig (Magdeburg) and Paul Gartner (Bucharest) for many fruitful collaborations. This work has strongly profited from the ongoing collaboration regarding state-of-the-art experiments in the groups of Peter Michler (Stuttgart), Manfred Bayer (Dortmund), Stephan Reitzenstein (Berlin), and Johnathan Finley (Munich). We are grateful for financial support from the Deutsche Forschungsgemeinschaft (DFG) and the Bundesministerium für Bildung und Forschung (BMBF).

References

1. J.P. Dowling, G.J. Milburn, Philos. Trans. R. Soc. Lond. A Math. Phys. Eng. Sci. **361**(1809), 1655 (2003). doi:10.1098/rsta.2003.1227, http://rsta.royalsocietypublishing.org/content/361/1809/1655
2. C. Roy, S. Hughes, Phys. Rev. X **1**(2), 021009 (2011). doi:10.1103/PhysRevX.1.021009
3. S. Schumacher, J. Förstner, A. Zrenner, M. Florian, C. Gies, P. Gartner, F. Jahnke, Opt. Express **20**(5), 5335 (2012). doi:10.1364/OE.20.005335, http://www.opticsexpress.org/abstract.cfm?URI=oe-20-5-5335
4. M. Florian, P. Gartner, C. Gies, F. Jahnke, New J. Phys. **15**(3), 035019 (2013). doi:10.1088/1367-2630/15/3/035019

5. M. Florian, A. Steinhoff, C. Gies, F. Jahnke, Appl. Phys. B **122**(1), 1 (2016). doi:10.1007/s00340-015-6296-5
6. S. Lichtmannecker, M. Florian, T. Reichert, M. Blauth, M. Bichler, F. Jahnke, J.J. Finley, C. Gies, M. Kaniber, arXiv:1602.03998 [cond-mat] (2016)
7. S. Ritter, P. Gartner, C. Gies, F. Jahnke, Opt. Express **18**(10), 9909 (2010). doi:10.1364/OE.18.009909
8. C. Gies, M. Florian, P. Gartner, F. Jahnke, Opt. Express **19**(15), 14370–14388 (2011). doi:10.1364/OE.19.014370
9. A. Steinhoff, P. Gartner, M. Florian, F. Jahnke, Phys. Rev. B **85**(20), 205144 (2012). doi:10.1103/PhysRevB.85.205144
10. H.J. Carmichael, *Statistical Methods in Quantum Optics 1: Master Equations and Fokker-Planck Equations (Theoretical and Mathematical Physics)* (Springer, Berlin, 2003)
11. L. Mandel, E. Wolf, *Optical Coherence and Quantum Optics* (Cambridge University Press, Cambridge, 1995)
12. C. Gardiner, P. Zoller, *Quantum Noise A Handbook of Markovian and Non-Markovian Quantum Stochastic Methods with Applications to Quantum Optics* (Springer, Berlin, 2004)
13. C. Gies, M. Florian, P. Gartner, F. Jahnke, in *Quantum Optics With Semiconductor Nanostructures*, ed. by F. Jahnke (Woodhead Publishing Limited, Sawston, 2012)
14. M. Kira, S.W. Koch, Phys. Rev. A **78**(2), 022102 (2008). doi:10.1103/PhysRevA.78.022102
15. W. Hoyer, M. Kira, S.W. Koch, in *Nonequilibrium Physics at Short Time Scales*, ed. by K. Morawetz (Springer, Berlin, 2004)
16. M. Florian, C. Gies, F. Jahnke, H.A.M. Leymann, J. Wiersig, Physical Review B **87**(16), 165306 (2013). doi:10.1103/PhysRevB.87.165306
17. H.A.M. Leymann, A. Foerster, J. Wiersig, Physical Review B **89**(8), 085308 (2014). doi:10.1103/PhysRevB.89.085308
18. M. Richter, A. Carmele, A. Sitek, A. Knorr, Phys. Rev. Lett. **103**(8), 087407 (2009). doi:10.1103/PhysRevLett.103.087407
19. A. Carmele, A. Knorr, M. Richter, Phys. Rev. B **79**(3), 035316 (2009). doi:10.1103/PhysRevB.79.035316
20. J. Wiersig, Phys. Rev. B **82**(15), 155320 (2010). doi:10.1103/PhysRevB.82.155320
21. S. Ates, C. Gies, S.M. Ulrich, J. Wiersig, S. Reitzenstein, A. Löffler, A. Forchel, F. Jahnke, P. Michler, Physical Review B **78**(15), 155319 (2008). doi:10.1103/PhysRevB.78.155319
22. M. Florian, C. Gies, P. Gartner, F. Jahnke, Journal of the Optical Society of America B **29**(2), A31 (2012). doi:10.1364/JOSAB.29.000A31
23. P. Michler, *Single Quantum Dots - Fundamentals, Applications and New Concepts* (Springer, Berlin, 2003)
24. P. Michler, A. Kiraz, C. Becher, W.V. Schoenfeld, P.M. Petroff, L. Zhang, E. Hu, A. Imamoglu, Science **290**, 2282 (2000)
25. M. Bajcsy, A. Majumdar, A. Rundquist, J. Vučković, New J. Phys. **15**(2), 025014 (2013). doi:10.1088/1367-2630/15/2/025014
26. C. Lang, D. Bozyigit, C. Eichler, L. Steffen, J.M. Fink, A.A. Abdumalikov, M. Baur, S. Filipp, M.P. da Silva, A. Blais, A. Wallraff, Phys. Rev. Lett. **106**(24), 243601 (2011). doi:10.1103/PhysRevLett.106.243601
27. C.S. Muñoz, E. del Valle, A.G. Tudela, K. Müller, S. Lichtmannecker, M. Kaniber, C. Tejedor, J.J. Finley, F.P. Laussy, Nat. Photonics **8**(7), 550 (2014). doi:10.1038/nphoton.2014.114
28. N. Somaschi, V. Giesz, L.D. Santis, J.C. Loredo, M.P. Almeida, G. Hornecker, S.L. Portalupi, T. Grange, C. Antón, J. Demory, C. Gómez, I. Sagnes, N.D. Lanzillotti-Kimura, A. Lemaítre, A. Auffèves, A.G. White, L. Lanco, P. Senellart, Nat. Photonics **10**(5), 340 (2016). doi:10.1038/nphoton.2016.23
29. M. Pelton, C. Santori, J. Vučković, B. Zhang, G.S. Solomon, J. Plant, Y. Yamamoto, Physical Review Letters **89**(23), 233602 (2002). doi:10.1103/PhysRevLett.89.233602
30. S. Buckley, K. Rivoire, J. Vučković, Rep. Progr. Phys. **75**(12), 126503 (2012). doi:10.1088/0034-4885/75/12/126503

31. J.L. O'Brien, A. Furusawa, J. Vučković, Nat. Photonics **3**(12), 687 (2009). doi:10.1038/nphoton.2009.229
32. M. Nomura, N. Kumagai, S. Iwamoto, Y. Ota, Y. Arakawa, Opt. Express **17**(18), 15975 (2009). doi:10.1364/OE.17.015975
33. S. Reitzenstein, C. Böckler, A. Bazhenov, A. Gorbunov, A. Löffler, M. Kamp, V.D. Kulakovskii, A. Forchel, Opt. Express **16**(7), 4848–4857 (2008). doi:10.1364/OE.16.004848
34. C. Gies, F. Jahnke, W.W. Chow, Physical Review A **91**(6), 061804 (2015). doi:10.1103/PhysRevA.91.061804
35. A. Predojevic, M. Jezek, T. Huber, H. Jayakumar, T. Kauten, G.S. Solomon, R. Filip, G. Weihs, Opt. Express **22**(4), 4789 (2014). doi:10.1364/OE.22.004789, http://www.opticsexpress.org/abstract.cfm?URI=oe-22-4-4789
36. G. Reithmaier, S. Lichtmannecker, T. Reichert, P. Hasch, K. Müller, M. Bichler, R. Gross, J.J. Finley, Sci. Rep. **3**, 1901 (2013). doi:10.1038/srep01901. PMID: 23712624 PMCID: PMC3664895
37. B. Calkins, P.L. Mennea, A.E. Lita, B.J. Metcalf, W.S. Kolthammer, A. Lamas-Linares, J.B. Spring, P.C. Humphreys, R.P. Mirin, J.C. Gates, P.G.R. Smith, I.A. Walmsley, T. Gerrits, S.W. Nam, Opt. Express **21**(19), 22657 (2013). doi:10.1364/OE.21.022657
38. F.E. Becerra, J. Fan, A. Migdall, Nat. Photonics **9**(1), 48 (2015). doi:10.1038/nphoton.2014.280
39. M. Bell, A. Antipov, B. Karasik, A. Sergeev, V. Mitin, A. Verevkin, IEEE Trans. Appl. Supercond. **17**(2), 289 (2007). doi:10.1109/TASC.2007.898616
40. *Single-Photon Generation and Detection: Physics and Applications* (Academic Press, Dublin, 2013). Google-Books-ID: gERMqvh2OjAC
41. R. Filip, L. Lachman, Physical Review A **88**(4), 043827 (2013). doi:10.1103/PhysRevA.88.043827
42. M. Nomura, N. Kumagai, S. Iwamoto, Y. Ota, Y. Arakawa, Nat. Phys. **6**, 279 (2010). doi:10.1038/nphys1518
43. H.J. Carmichael, *Statistical Methods in Quantum Optics 2: Non-Classical Fields*, 2008th edn. (Springer, Berlin, 2007)
44. T. Yoshie, A. Scherer, J. Hendrickson, G. Khitrova, H.M. Gibbs, G. Rupper, C. Ell, O.B. Shchekin, D.G. Deppe, Nature **432**(7014), 200 (2004). doi:10.1038/nature03119
45. J.P. Reithmaier, G. Sk ek, A. Löffler, C. Hofmann, S. Kuhn, S. Reitzenstein, L.V. Keldysh, V.D. Kulakovskii, T.L. Reinecke, A. Forchel, Nature **432**(7014), 197 (2004). doi:10.1038/nature02969
46. F. Gericke, C. Gies, P. Gartner, S. Holzinger, C. Hopfmann, T. Heindel, J. Wolters, C. Schneider, M. Florian, F. Jahnke, S. Höfling, M. Kamp, S. Reitzenstein, arXiv:1606.05591 [cond-mat, physics:physics] (2016)
47. W.W. Chow, F. Jahnke, C. Gies, Light Sci. Appl. **3**(8), e201 (2014). doi:10.1038/lsa.2014.82
48. N. Sangouard, C. Simon, N. Gisin, J. Laurat, R. Tualle-Brouri, P. Grangier, J. Opt. Soc. Am. B **27**(6), A137 (2010). doi:10.1364/JOSAB.27.00A137
49. A.K. Ekert, Phys. Rev. Lett. **67**(6), 661 (1991). doi:10.1103/PhysRevLett.67.661
50. B.D. Gerardot, S. Seidl, P.A. Dalgarno, R.J. Warburton, D. Granados, J.M. Garcia, K. Kowalik, O. Krebs, K. Karrai, A. Badolato, P.M. Petroff, Appl. Phys. Lett. **90**(4), 041101 (2007). doi:10.1063/1.2431758
51. S. Bounouar, M. Müller, A.M. Barth, M. Glässl, V.M. Axt, P. Michler, Phys. Rev. B **91**(16), 161302 (2015). doi:10.1103/PhysRevB.91.161302
52. Y. Ota, S. Iwamoto, N. Kumagai, Y. Arakawa, Phys. Rev. Lett. **107**(23), 233602 (2011). doi:10.1103/PhysRevLett.107.233602
53. C.A. Kessler, M. Reischle, F. Hargart, W.M. Schulz, M. Eichfelder, R. Roßbach, M. Jetter, P. Michler, P. Gartner, M. Florian, C. Gies, F. Jahnke, Phys. Rev. B **86**(11), 115326 (2012). doi:10.1103/PhysRevB.86.115326
54. G. Lindblad, Commun. Math. Phys. **48**(2), 119 (1976). doi:10.1007/BF01608499
55. H.P. Breuer, *The Theory of Open Quantum Systems* (Oxford University Press, USA, 2007)

56. A. Steinhoff, H. Kurtze, P. Gartner, M. Florian, D. Reuter, A.D. Wieck, M. Bayer, F. Jahnke, Phys. Rev. B **88**(20), 205309 (2013). doi:10.1103/PhysRevB.88.205309
57. T.S. Sosnowski, T.B. Norris, H. Jiang, J. Singh, K. Kamath, P. Bhattacharya, Phys. Rev. B **57**, R9423 (1998)
58. J. Urayama, T.B. Norris, J. Singh, P. Bhattacharya, Phys. Rev. Lett. **86**, 4930 (2001). doi:10.1103/PhysRevLett.86.4930
59. F. Quochi, M. Dinu, N.H. Bonadeo, J. Shah, L.N. Pfeiffer, K.W. West, P.M. Platzman, Phys. B **314**, 263 (2002). doi:10.1016/S0921-4526(01)01383-7
60. F. Quochi, M. Dinu, L.N. Pfeiffer, K.W. West, C. Kerbage, R.S. Windeler, B.J. Eggleton, Phys. Rev. B **67**, 235323 (2003). doi:10.1103/PhysRevB.67.235323
61. P. Borri, W. Langbein, U. Woggon, V. Stavarache, D. Reuter, A.D. Wieck, Phys. Rev. B **71**(11), 115328 (2005). doi:10.1103/PhysRevB.71.115328
62. H. Kurtze, J. Seebeck, P. Gartner, D.R. Yakovlev, D. Reuter, A.D. Wieck, M. Bayer, F. Jahnke, Phys. Rev. B **80**(23), 235319 (2009). doi:10.1103/PhysRevB.80.235319
63. A. Laucht, M. Kaniber, A. Mohtashami, N. Hauke, M. Bichler, J.J. Finley, Phys. Rev. B **81**, 241302 (2010). doi:10.1103/PhysRevB.81.241302
64. U. Bockelmann, T. Egeler, Phys. Rev. B **46**, 15574 (1992). doi:10.1103/PhysRevB.46.15574
65. T. Inoshita, H. Sakaki, Phys. Rev. B **46**, 7260 (1992). doi:10.1103/PhysRevB.46.7260
66. I. Vurgaftman, Y. Lam, J. Singh, Phys. Rev. B **50**, 14309 (1994). doi:10.1103/PhysRevB.50.14309
67. A.L. Efros, V.A. Kharchenko, M. Rosen, Solid State Commun. **93**, 281 (1995)
68. T. Inoshita, H. Sakaki, Phys. Rev. B **56**, 4355 (1997). doi:10.1103/PhysRevB.56.R4355
69. A.V. Uskov, F. Adler, H. Schweizer, M.H. Pilkuhn, J. Appl. Phys. **81**, 7895 (1997). doi:10.1063/1.365363
70. M. Brasken, M. Lindberg, M. Sopanen, H. Lipsanen, J. Tulkki, Phys. Rev. B **58**, 15993 (1998). doi:10.1103/PhysRevB.58.R15993
71. H. Jiang, J. Singh, IEEE J. Quantum Electron. **34**, 1188 (1998)
72. R. Ferreira, G. Bastard, Appl. Phys. Lett. **74**, 2818 (1999). doi:10.1063/1.124024
73. T. Stauber, R. Zimmermann, H. Castella, Phys. Rev. B **62**, 7336 (2000). doi:10.1103/PhysRevB.62.7336
74. K. Lüdge, M.J.P. Bormann, E. Malić, P. Hövel, M. Kuntz, D. Bimberg, A. Knorr, E. Schöll, Phys. Rev. B **78**(3), 035316 (2008). doi:10.1103/PhysRevB.78.035316
75. M. Grundmann, D. Bimberg, physica status solidi (a) **164**(1), 297–300 (1997). doi:10.1002/1521-396X(199711)164:1<297::AID-PSSA297>3.0.CO;2-5
76. P. Borri, V. Cesari, W. Langbein, Phys. Rev. B **82**(11), 115326 (2010). doi:10.1103/PhysRevB.82.115326
77. J.I. Climente, A. Bertoni, M. Rontani, G. Goldoni, E. Molinari, Phys. Rev. B **74**(12), 125303 (2006). doi:10.1103/PhysRevB.74.125303
78. G.D. Mahan, *Many Particle Physics*, 3rd edn (Springer, Berlin, 2000)
79. U. Bockelmann, G. Bastard, Phys. Rev. B **42**, 8947 (1990). doi:10.1103/PhysRevB.42.8947
80. H. Benisty, C.M. Sotomayor-Torres, C. Weisbuch, Phys. Rev. B **44**, 10945 (1991). doi:10.1103/PhysRevB.44.10945
81. L. Besombes, K. Kheng, L. Marsal, H. Mariette, Phys. Rev. B **63**(15), 155307 (2001). doi:10.1103/PhysRevB.63.155307
82. P. Borri, W. Langbein, S. Schneider, U. Woggon, R.L. Sellin, D. Ouyang, D. Bimberg, Phys. Rev. Lett. **87**(15), 157401 (2001), http://link.aps.org/abstract/PRL/v87/e157401
83. S. Schmitt-Rink, D.A.B. Miller, D.S. Chemla, Phys. Rev. B **35**(15), 8113 (1987). doi:10.1103/PhysRevB.35.8113
84. T. Takagahara, Phys. Rev. B **60**(4), 2638 (1999). doi:10.1103/PhysRevB.60.2638
85. B. Krummheuer, V.M. Axt, T. Kuhn, Phys. Rev. B **65**(19), 195313 (2002). doi:10.1103/PhysRevB.65.195313
86. R. Zimmermann, E. Runge, Proceedings of the 26th ICPS (Edinburgh, 2002)
87. E. Pazy, Semicond. Sci. Technol. **17**(11), 1172 (2002). doi:10.1088/0268-1242/17/11/307

88. P. Borri, W. Langbein, S. Schneider, U. Woggon, R.L. Sellin, D. Ouyang, D. Bimberg, Phys. Rev. Lett. **89**(18), 187401 (2002). doi:10.1103/PhysRevLett.89.187401
89. H. Gotoh, H. Kamada, T. Saitoh, H. Ando, J. Temmyo, Phys. Rev. B **69**(15), 155328 (2004). doi:10.1103/PhysRevB.69.155328
90. G. Moody, R. Singh, H. Li, I.A. Akimov, M. Bayer, D. Reuter, A.D. Wieck, S.T. Cundiff, Phys. Rev. B **87**(4), 045313 (2013). doi:10.1103/PhysRevB.87.045313
91. S. Strauf, K. Hennessy, M.T. Rakher, Y.S. Choi, A. Badolato, L.C. Andreani, E.L. Hu, P.M. Petroff, D. Bouwmeester, Phys. Rev. Lett. **96**, 127404 (2006). doi:10.1103/PhysRevLett.96.127404
92. S.M. Ulrich, C. Gies, J. Wiersig, S. Reitzenstein, C. Hofmann, A. Löffler, A. Forchel, F. Jahnke, P. Michler, Phys. Rev. Lett. **98**, 043906 (2007)
93. I. Wilson-Rae, A. Imamoglu, Phys. Rev. B **65**(23), 235311 (2002). doi:10.1103/PhysRevB.65.235311
94. D. Press, S. Götzinger, S. Reitzenstein, C. Hofmann, A. Löffler, M. Kamp, A. Forchel, Y. Yamamoto, Phys. Rev. Lett. **98**(11), 117402 (2007). doi:10.1103/PhysRevLett.98.117402
95. G. Tarel, V. Savona, physica status solidi (c) **6**(4), 902 (2009). doi:10.1002/pssc.200880577
96. M. Kaniber, A. Laucht, A. Neumann, J.M. Villas-Bôas, M. Bichler, M.C. Amann, J.J. Finley, Phys. Rev. B **77**(16), 161303 (2008). doi:10.1103/PhysRevB.77.161303
97. S. Ates, S.M. Ulrich, A. Ulhaq, S. Reitzenstein, A. Löffler, S. Höfling, A. Forchel, P. Michler, Nat. Photonics **3**(12), 724 (2009). doi:10.1038/nphoton.2009.215
98. U. Hohenester, A. Laucht, M. Kaniber, N. Hauke, A. Neumann, A. Mohtashami, M. Seliger, M. Bichler, J.J. Finley, Phys. Rev. B **80**(20), 201311 (2009). doi:10.1103/PhysRevB.80.201311
99. D. Dalacu, K. Mnaymneh, V. Sazonova, P.J. Poole, G.C. Aers, J. Lapointe, R. Cheriton, A.J. SpringThorpe, R. Williams, Phys. Rev. B **82**(3), 033301 (2010). doi:10.1103/PhysRevB.82.033301
100. M. Calic, P. Gallo, M. Felici, K.A. Atlasov, B. Dwir, A. Rudra, G. Biasiol, L. Sorba, G. Tarel, V. Savona, E. Kapon, Phys. Rev. Lett. **106**(22), 227402 (2011). doi:10.1103/PhysRevLett.106.227402
101. A. Majumdar, E.D. Kim, Y. Gong, M. Bajcsy, J. Vučković, Phys. Rev. B **84**(8), 085309 (2011). doi:10.1103/PhysRevB.84.085309
102. U. Hohenester, Phys. Rev. B **81**(15), 155303 (2010). doi:10.1103/PhysRevB.81.155303
103. D.P.S. McCutcheon, A. Nazir, New J. Phys. **12**(11), 113042 (2010). doi:10.1088/1367-2630/12/11/113042, http://stacks.iop.org/1367-2630/12/i=11/a=113042
104. A. Würger, Phys. Rev. B **57**(1), 347 (1998). doi:10.1103/PhysRevB.57.347
105. J.D. Joannopoulos, P.R. Villeneuve, S. Fan, Nature **386**(6621), 143 (1997). doi:10.1038/386143a0
106. S. Noda, M. Fujita, T. Asano, Nat. Photonics **1**(8), 449 (2007). doi:10.1038/nphoton.2007.141
107. S. Strauf, F. Jahnke, Laser Photonics Rev. **5**(5), 607 (2011). doi:10.1002/lpor.201000039
108. E. Dekel, D. Gershoni, E. Ehrenfreund, D. Spektor, J.M. Garcia, P.M. Petroff, Phys. Rev. Lett. **80**(22), 4991 (1998). doi:10.1103/PhysRevLett.80.4991
109. M. Winger, T. Volz, G. Tarel, S. Portolan, A. Badolato, K.J. Hennessy, E.L. Hu, A. Beveratos, J. Finley, V. Savona, A. Imamoğlu, Phys. Rev. Lett. **103**(20), 207403 (2009). doi:10.1103/PhysRevLett.103.207403
110. H. Leymann, A. Foerster, F. Jahnke, J. Wiersig, C. Gies, Phys. Rev. Appl. **4**(4), 044018 (2015). doi:10.1103/PhysRevApplied.4.044018
111. E. Mascarenhas, D. Gerace, M.F. Santos, A. Auffèves, Phys. Rev. A **88**(6), 063825 (2013). doi:10.1103/PhysRevA.88.063825
112. K. Karrai, R.J. Warburton, C. Schulhauser, A. Högele, B. Urbaszek, E.J. McGhee, A.O. Govorov, J.M. Garcia, B.D. Gerardot, P.M. Petroff, Nature **427**(6970), 135 (2004). doi:10.1038/nature02109
113. N. Chauvin, C. Zinoni, M. Francardi, A. Gerardino, L. Balet, B. Alloing, L.H. Li, A. Fiore, Phys. Rev. B **80**(24), 241306 (2009). doi:10.1103/PhysRevB.80.241306

114. M. Florian, P. Gartner, A. Steinhoff, C. Gies, F. Jahnke, Phys. Rev. B **89**(16), 161302(R) (2014). doi:10.1103/PhysRevB.89.161302
115. M. Gross, S. Haroche, Phys. Rep. **93**(5), 301 (1982). doi:10.1016/0370-1573(82)90102-8
116. T. Brandes, Phys. Rep. **408**(5–6), 315 (2005). doi:10.1016/j.physrep.2004.12.002
117. M. Scheibner, T. Schmidt, L. Worschech, A. Forchel, G. Bacher, T. Passow, D. Hommel, Nat. Phys. **3**(2), 106 (2007). doi:10.1038/nphys494
118. M. Kozub, L. Pawicki, P. Machnikowski, Phys. Rev. B **86**(12), 121305 (2012). doi:10.1103/PhysRevB.86.121305
119. J.A. Mlynek, A.A. Abdumalikov, C. Eichler, A. Wallraff, Nature Communications **5** (2014). doi:10.1038/ncomms6186
120. J.G. Bohnet, Z. Chen, J.M. Weiner, D. Meiser, M.J. Holland, J.K. Thompson, Nature **484**(7392), 78 (2012). doi:10.1038/nature10920
121. G. Timothy, Noe Ii, J.H. Kim, J. Lee, Y. Wang, A.K. Wójcik, S.A. McGill, D.H. Reitze, A.A. Belyanin. J. Kono Nat. Phys. **8**(3), 219 (2012). doi:10.1038/nphys2207
122. V.V. Temnov, U. Woggon, Opt. Express **17**, 5774 (2009). doi:10.1364/OE.17.005774
123. A. Auffèves, D. Gerace, S. Portolan, A. Drezet, M.F. Santos, New J. Phys. **13**(9), 093020 (2011). doi:10.1088/1367-2630/13/9/093020
124. F. Jahnke, C. Gies, M. Aßmann, M. Bayer, H.a.M. Leymann, A. Foerster, J. Wiersig, C. Schneider, M. Kamp, S. Höfling, Nat. Commun. **7**, 11540 (2016). doi:10.1038/ncomms11540
125. D. Meiser, M.J. Holland, Physical Review A **81**(6), 063827 (2010). doi:10.1103/PhysRevA.81.063827
126. G. Björk, Y. Yamamoto, IEEE J. Quantum Electron. **27**, 2386 (1991). doi:10.1109/3.100877
127. H. Yokoyama, S.D. Brorson, J. Appl. Phys. **66**, 4801 (1989). doi:10.1063/1.343793

http://www.springer.com/978-3-319-56377-0

Quantum Dots for Quantum Information Technologies

Michler, P. (Ed.)
2017, XVII, 448 p. 221 illus., 80 illus. in color.,
Hardcover
ISBN: 978-3-319-56377-0